Indian Head Division
Naval Surface Warfare Center
Indian Head, MD 20640-5035

IHTR 1914
30 December 1999

DYNAMIC LOADING OF POROUS INERT AND ENERGETIC MATERIALS

H.W. Sandusky
B.C. Glancy
R.R. Bernecker

Indian Head Division
Naval Surface Warfare Center

A.D. Krall

Advanced. Technology and Research, Inc.

REPORT DOCUMENTATION PAGE

Form Approved
QMB No. 0704-0188

Public reporting burden for this collection of information is estimated to average 1 hour per response, including the time for reviewing instructions, searching existing data sources, gathering and maintaining the data needed, and completing and reviewing the collection of information. Send comments regarding the burden estimate or any other aspect of this collection of information, including suggestion for reducing this burden, to Washington Headquarters Services, Directorate for Information Operations and Reports. 1215 Jefferson Davis Highway, Suite 1204, Arlington, VA 22202-4302, and to the Office of Management and Budget, Paperwork Reduction project (0704-0188), Washington, DC 20503.

1. AGENCY USE ONLY (*Leave Blank*)

2. REPORT DATE
30 December 1999

3. REPORT TYPE AND DATES COVERED
Final Report

4. TITLE AND SUBTITLE
DYNAMIC LOADING OF POROUS INERT AND ENERGETIC MATERIALS

5. FUNDING NUMBERS

6. AUTHOR(S)
H.W. Sandusky, B.C. Glancy, R.R. Bernecker, Indian Head Division, Naval Surface Warfare Center
A.D. Krall, Advanced Technology and Research, Inc

7. PERFORMING ORGANIZATIONS NAME(S) AND ADDRESS(ES)
Indian Head Division
Naval Surface Warfare Center
Indian Head, MD 20640-5035

8. PERFORMING ORGANIZATION REPORT NUMBER
IHTR 1914

9. SPONSORING/MONITORING AGENCY NAME(S) AND ADDRESS(ES)

Strategic Systems Programs
3801 Nebraska Ave., NE
Washington, DC 20393-5466

Office of Naval Research
800 N. Quincy St.
Arlington, VA 22217-5660

10. SPONSORING/MONITORING AGENCY REPORT NUMBER

11. SUPPLEMENTARY NOTES

12a. DISTRIBUTION/AVAILABILITY STATEMENT
Approved for public release; distribution is unlimited.

12b. DISTRIBUTION CODE

13. ABSTRACT (*Maximum 200 words*)

Bed compaction occurs throughout the various stages of deflagration-to-detonation transition (DDT). As burning begins, compressive waves compact the adjacent porous bed, thereby restricting gas flow and increasing the pressure buildup. Stronger compressive waves coalesce into a compaction front, where rapid pore collapse creates hot spots and initiates compressive reaction. Rapid growth of compressive reaction will strengthen the compaction front into a shock wave that can then transit to detonation. Experimental techniques were developed for driving quasi-steady fronts into porous beds at pressures of interest to DDT, ranging from 15 to 500 MPa. A variety of explosives and propellants were studied, along with some inert materials to avoid any influence from reaction. Measurements were made during the compaction process of the front velocity, the state of the compacted bed behind the front in the absence of reaction, the time for the onset of compressive reaction, the pressure growth and increased front velocity from reaction, and the time and distance to detonation. These data were related to DDT experiments on some of the same materials. At the highest impact pressures, distance-to-detonation measurements for coarse tetryl were similar to published wedge test data.

14. SUBJECT TERMS
Piston driven compaction
Deflagration-to-detonation transition

15. NUMBER OF PAGES
62

16. PRICE CODE

17. SECURITY CLASSIFICATION OF REPORT	18. SECURITY CLASSIFICATION OF THIS PAGE	19. SECURITY CLASSIFICATION OF ABSTRACT	20. LIMITATION OF ABSTRACT
UNCLASSIFIED	UNCLASSIFIED	UNCLASSIFIED	SAR

This page intentionally left blank.

FOREWORD

The sensitivity of energetic materials to transit to detonation increases considerably with extensive porosity (>10%) because of the vigorous reaction that can occur as the pores collapse. The strength of energetic materials is such that confined burning, or weak shock loading, with pressures <100 MPa (one kilobar), will collapse pores. In deflagration-to-detonation transition (DDT), the front of the confined burning does not continuously accelerate by convection through pores and transit to detonation, because compressive waves from the burning propagate ahead of that front and collapse the pores. Hot spot (compressive) reaction from pore collapse was widely recognized as an ignition source for shock-to-detonation transition (SDT). Only more recently has compressive reaction in DDT been recognized as the driver for the rapid pressure buildup prior to SDT. Since this phenomenon was not well understood, a variety of experiments were conducted in which porous beds of inerts, explosives, and propellants were dynamically loaded in a controlled manner with pressures ranging from <15 to >500 MPa. These pressures covered the range of output from an ignitor in a DDT experiment to the low amplitude shock prior to SDT. Measurements were made of dynamic compaction, compressive reaction, and shock buildup to detonation.

This report reviews the various dynamic loading experiments, which were conducted over a ten-year period at the former White Oak Laboratory of the Naval Surface Warfare Center (NSWC). Many of the experiments are documented in detail in the provided references. These studies were funded by the Independent Research program at this Center, the Office of Naval Research 6.2 Explosives Block, and the High-Energy Propellant Safety and Hazard Assessment of Rocket Propellants programs sponsored by Strategic Systems Programs.

This work was part of a collaborative study that included the quasi-static experiments of Wayne Elban and Paul Coyne, Jr. at Loyola College and the development of numerical models, principally by Doug Kooker at the Army Research Laboratory, Mel Bear at the Sandia National Laboratory, Chan Price at the Naval Air Warfare Center, Al Weston at the Lawrence Livermore National Laboratory, and Kibong Kim at NSWC. The authors greatly appreciate the contributions of these investigators, especially Doug Kooker for organizing and documenting the JANNAF workshops at which experimental data and model predictions were compared. Special appreciation goes to Sigmund Jacobs, who assisted and reviewed various aspects of the work. The infrared emission measurements in one experiment on WC 231 ball powder were made by Phil Miller, then at NSWC. The many experiments were performed with the technical assistance of Carl Groves, Reggie McNair, and Patrick Femiano. The electronic flash system that provided the illumination for high-speed photography was made by Nick Vogle, who along with Harry Cleaver developed and maintained other electronic instrumentation for the experiments.

Approved and released by:

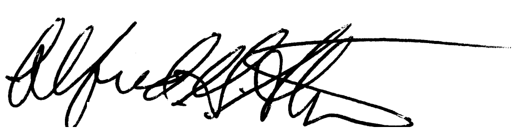

Dr. Alfred G. Stern
Director, Chemistry and Detonics Division

This page intentionally left blank.

CONTENTS

Tables

Figures

Figures—*Continued*

Heading *Page*

INTRODUCTION

Porosity is required for deflagration-to-detonation transition (DDT) to occur, except for very shock sensitive cast materials. The primary consideration of porosity in early DDT investigations involved the permeability of the porous bed, which would permit the convective transfer of hot combustion products for more rapidly spreading ignition. While convective burning was necessary for a rapid pressure buildup, the investigations of Bernecker and Price showed that an accelerating convective ignition front did not itself develop into a shock that would transit to detonation.[1,2] They found that compressive waves from accelerated burning near the ignitor would coalesce into a strong compressive wave (SCW). The SCW would initiate additional reaction, referred to as compressive burning, which strengthened the SCW into a shock that could transit to detonation. Although dynamic compaction of the porous bed by the compressive waves was not directly observed in the steel tube experiments, supersonic velocities for the SCW in 91/9 RDX/wax beds packed at less than 78% of theoretical maximum density (TMD) indicated that these beds had been compacted by the early burning.[1] Russian investigators[3] had measured a higher retonation (rearward detonation) than detonation velocity during DDT in porous PETN, also indicating compaction of the predetonation column. With the inclusion of flash radiography in plastic tube DDT experiments, Bernecker and coworkers observed the formation of a fully compacted plug between the burning near the ignitor and the downstream transition to detonation.[4] It was subsequently demonstrated by Green and co-workers that dynamic compaction of a porous high-energy propellant by a piston would initiate compressive reaction and similarly result in a transition to detonation.[5]

The objectives of the presented work were to investigate the dynamic compaction of porous beds and the compressive reaction that results from compaction, and to provide insight into and quantitative data for modeling DDT. While dynamic compaction has several roles during DDT, the onset and growth of compressive reaction is particularly important to the final buildup to detonation and was one of the least understood DDT processes at the onset of the investigation. Compressive reaction begins at the compaction front as hot spots are created by rapid deformation of material that surrounds the collapsing pores. Localized heating from high strain deformation is responsible for initiation of reaction in drop-weight impact and fragment penetration as well as DDT. In all these tests, the threshold of reaction occurs at similar bulk rates of deformation (80-200 m/s) for a variety of materials.[6] When a pressure gradient exists, such as in the radial pressure during drop-weight impact, threshold reaction occurs in the low pressure zone where the deformation is the greatest. It appears, therefore, that the primary role of pressure in hot spot reactions is to drive the deformation.

Dynamic compaction of porous beds was studied by various means to simulate the wide range of pressures and pressurization rates during DDT.[4] Initial studies were conducted using the ignitors from the DDT experimental arrangement to compact porous inert materials and thereby simulate compaction during the early stages of DDT.[7-9] For similar studies on energetic materials, the hot gases from the ignitor were replaced by pressurized nitrogen from a closely coupled reservoir. These experiments were referred to as cold gas compaction (CGC) since the nitrogen was below ambient temperature as it expanded out of the reservoir. CGC experiments were conducted on inerts and ball propellants.[7,10,11] Both ignitor driven compaction (IDC) and CGC experiments produced pressures in the range of only 10 to 20 MPa, corresponding to the pre-ignition stage of DDT. To examine compaction throughout the early stages of DDT, porous beds were impacted by a long piston propelled from a powder gun. Piston driven compaction (PDC) produced a long duration (~200 μs) pressure pulse, which resulted in a quasi-steady wave propagating in the porous bed. Dynamic compaction measurements with the PDC apparatus were obtained for inerts,[9-11] HMX powders,[11] granulated plastic-bonded explosives (PBXs),[11] ball propellants,[12-14] a casting powder for a high-energy propellant,[15] and shreds of a high-energy propellant.[16] A quasi-steady compaction experiment was easier to analyze than the ramping of coalescing compressive waves that occurs in DDT; however, each PDC experiment resulted in compaction measurements at only one pressure or over a narrow range of pressures. Liddiard developed an apparatus for ramp loading a porous bed and conducted a successful experiment on an inert material.[10,11] He also dynamically compacted a porous inert with the shock from a gap test donor.[10,11]

Dynamic compaction studies were complemented by quasi-static experiments, which were essential for several reasons. First, a single quasi-static experiment can provide a complete profile of load versus extent of compaction, which would require a series of dynamic experiments. Second, quasi-static experiments do not initiate reaction in energetic materials and thus the mechanical response of the porous bed can be studied independently of material decomposition. Finally, samples that are compacted quasi-statically can be recovered for subsequent analysis. At this Center, Elban and coworkers machine-pressed many of the same materials with a double-acting ram in a thick-wall steel tube. Quasi-static measurements of average stress versus bed density were obtained for inerts,[8,10,17] HMX powders (as-manufactured and several sieve cuts),[18,19] five ball propellants,[12,20] two particle sizes of a casting powder for a high-energy propellant,[21] and shreds of a high-energy propellant.[16] In later quasi-static experiments on HMX,[22] a casting powder for a high-energy propellant,[22] and ball propellants,[23] radial stress measurements were also obtained so that the stress tensor could be evaluated. Coyne and coworkers at this Center developed a strain rate sensitivity model that used stress relaxation measurements following quasi-static compaction in order to extrapolate quasi-static data to dynamic strain rates for an inert,[24] HMX,[25] and ball propellants.[26] Atwood and coworkers at the Naval Air Warfare Center (NAWC) used a single ram to compact some of the same ball propellants and then measured gas permeability in the compacted beds.[27] Various particle sizes of HMX were isostatically compacted by Costantino and Tao at the Lawrence Livermore National Laboratory (LLNL).[28]

The quasi-static load/compaction dependence was modeled for plastically deforming, primarily spherical, ball propellants.[29] This model assumed that the spheres were packed in cubic lattices, and that the contact sites between particles deformed to accommodate the average bed stress. Other than the packing arrangement, the only parameter required for the model was the interparticle stress over the contact areas, which was assumed to be the Meyers yield stress. The model applied to most of the compaction range, from the initial state when particles are undeformed until the pores are isolated. This corresponds to a range of 40% to 10% porosity for a simple cubic lattice. Pore isolation occurs as the adjacent contact areas on a particle become large enough to impinge. Once this occurs, further compaction can be approximated as the collapse of hollow spheres within a matrix of solid material, using the model of Carroll and Holt.[30] Since porous beds are seldom packed as simple, body-centered, or face-centered cubic lattices, the lattice compaction model accounted for the initial porosity of an actual bed by assuming either a mixture of simple and face-centered cubic lattices or an average number of contacts per particle.

Compressive reaction was observed for ball propellants when dynamically compacted with nitrogen at pressures less than 20 MPa.[15,31] However, most compressive reaction studies were conducted with the PDC arrangement because it could produce bed pressures that correspond to the SCW during the onset of the final stages of DDT. Also, the quasi-steady wave in the PDC experiment permits the association of an ignition delay and subsequent rate of reaction growth with a specific compaction wave strength. Compressive reaction studies were conducted on coarse tetryl and all of the energetic materials that had been compacted with the PDC apparatus.[12-15,31-32] Use of the apparatus was extended to dynamic loadings corresponding to low amplitude shocks in the range of 100 to 500 MPa.[33] It was possible, for example, to achieve the lower shock pressures used by Lindstrom in wedge tests on 75.1% TMD coarse tetryl.[34]

Both dynamic compaction and compressive reaction experiments were modeled. Dynamic compaction models contained constitutive relations based on quasi-static data. In addition to individual efforts (e.g., References 8,35,36), there was a JANNAF sponsored workshop on numerically predicting dynamic compaction.[37] In a subsequent workshop, the modelers shared their predictions for the onset and growth of compressive reaction in PDC experiments on ball propellants.[38] Other reports on modeling compressive reaction in PDC experiments appear in References 39 to 42.

Many of the results from the dynamic loading studies have been documented and will only be summarized in this report. Recent dynamic compaction as well as compressive reaction data that have not been previously reported will be discussed in detail. These recent studies utilized a microwave interferometer for measuring particle and front velocities[43] and for providing an estimate of hot spot concentration.[44,45]

EXPERIMENTAL APPROACH

PDC Apparatus

Much of the data to be discussed in this report were obtained with the PDC apparatus shown in Figure 1. The experimental arrangement used a powder gun to propel a 25.4-mm-diameter piston into a tube that confined the porous bed. The powder charge for propelling the piston consists of a DDT ignitor and up to 5.5 grams of ball powder. Most compaction and compressive reaction experiments utilized a 305-mm-long Lexan piston. For the higher piston velocities (>300 m/s) required for low amplitude shock initiation, the Lexan pistons yielded excessively upon bed impact. This was corrected in the final experiments by using 127-mm-long aluminum pistons, which were propelled from a shorter barrel. The barrel extender shown in Figure 1 was incorporated because violent reactions caused some expansion of the end of the barrel. Better protection of the barrel was obtained with Lexan versus steel extenders. The barrel extender and confining tube were clamped together between steel plates by four 19-mm threaded rods. Slots in the barrel extender served several purposes, one of which was to vent the air between the piston and the porous bed. Air injection into the bed was further prevented by an ~0.8-mm-thick plastic disk on the end of the bed; that disk also kept the bed from spilling or springing out of the tube during setup.

Another purpose for the slots in the barrel extender was to permit high-speed camera measurements of the piston velocity before and after impacting the bed. To accomplish this, the piston was circumferentially scribed and illuminated by an electronic flash. Transparent Lexan pistons were backlit with a linear xenon tube (50-mm-long arc length by 6-mm-diameter bore) that was custom ordered from Genesis Lamp Corp. Aluminum pistons were frontlit with an inexpensive Radio Shack xenon tube (catalog number 272-1145). The same flash circuit was used for both tubes and consisted of a 600-μF capacitor charged to 600-1000 VDC and an EG&G TM-12A trigger module for series injection triggering. The electronic flash unit was triggered by the piston contacting a shorting pin ~50 mm before the beginning of the slots in the barrel extender. For the slower piston velocities (<200 m/s), the triggering of the flash unit was delayed after the pin shorted so that the useful illumination from the flash (~2 ms) occurred closer to bed impact.

Different tubes were used to contain the porous bed depending on the instrumentation, confinement, and type of experiment. All tubes had an inner diameter only slightly larger (generally <0.1 mm) than the 25.4-mm-diameter piston to avoid extrusion of the compacting material between the piston and tube wall. Cross sections of the various tubes are shown in Figure 2. Transparent Lexan tubes (Figure 2a) with ~25-mm-thick walls permitted both high-speed photographic and flash radiographic measurements, but provided only low confinement for the bed. Some increase of confinement for one-dimensional (1-D) compaction measurements with flash radiography were obtained with the aluminum tubes in Figures 2b and 2c. The thin (~3.2 mm) aluminum walls in these intermediate confinement arrangements failed quickly once compressive reaction began, thus extinguishing the reaction. This was advantageous for preserving the rest of the apparatus from violent reactions, but did not allow any observations of the growth of compressive reaction. In the low confinement of the plastic tubes, transitions to detonation from compressive reaction were observed for the more shock sensitive energetic materials, while in other materials there was not even the onset of compressive reaction. Thick-wall (~25 mm) tubes of mild steel (C1018), like that in Figures 1 and 2d, were used to provide high confinement for 1-D measurements of compressive reaction and low amplitude shock initiation. In one experiment, a high strength steel (HSS, hardened 4340) was used because of the suspicion that even a regular steel tube provided marginal confinement in some low amplitude shock initiation measurements.

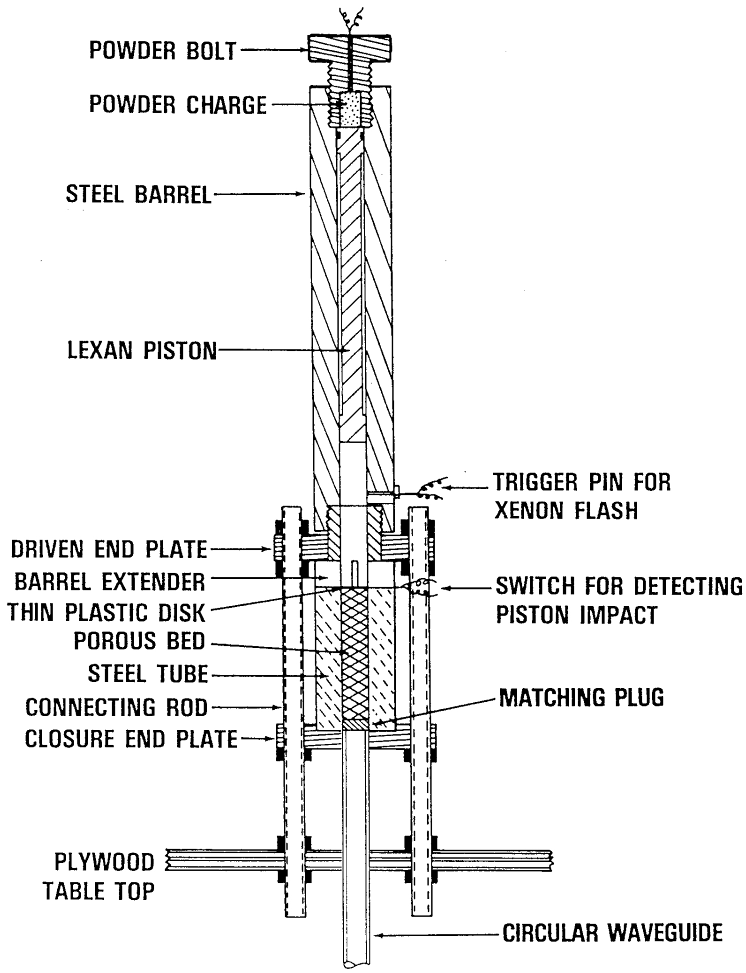

Figure 1. PDC Apparatus Interfaced with Microwave Interferometer

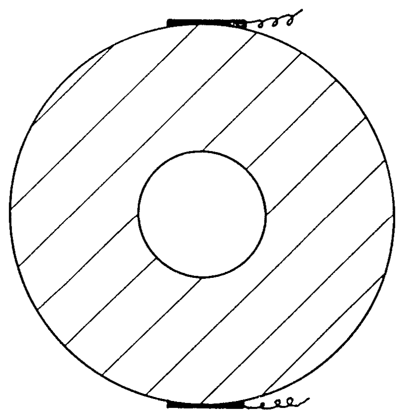

a. Lexan tube (75.6 mm OD) with circumferentially mounted strain gauges

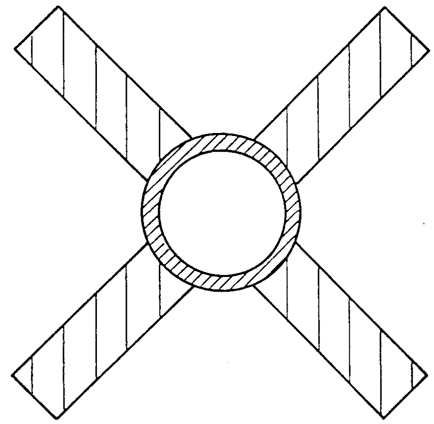

b. Steel-supported aluminum tube (31.8 mm OD) for flash radiography

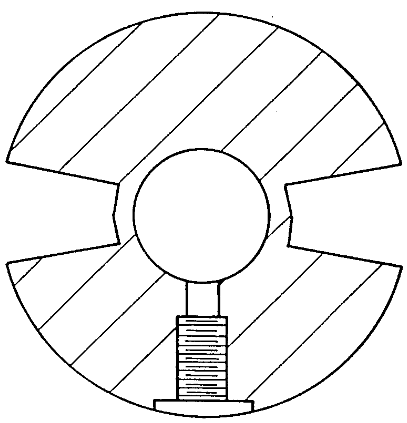

c. Aluminum tube (75.6 mm OD) with pressure transducer mounts and cutouts for radiography

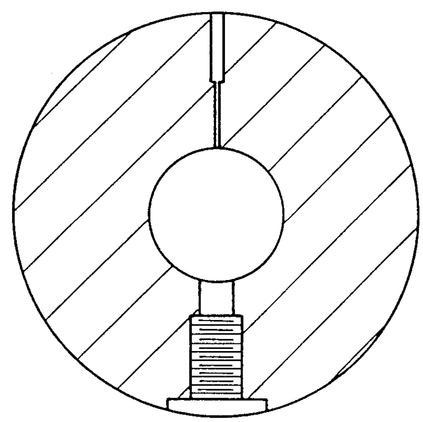

d. Steel tube (75.6 mm OD) with holes for probes and mounts for transducers

Figure 2. Cross Sections of Various Confinement Tubes (25.4-mm ID) for PDC Experiments

Instrumentation

High-speed photography was the primary instrumentation in Lexan tube experiments. In both Lexan and steel tube experiments, photography was used to measure piston velocity before and after bed impact, as described above. A camera was not used in the intermediate confinement (aluminum tube) experiments for dynamic compaction because the important measurement of piston velocity after bed impact was precisely obtained with flash radiography. A Cordin model 136A streak camera was used for most photographic measurements; in some preliminary Lexan tube experiments, a Cordin model 375 framing camera was used to obtain full field views of tube deformation as well as record the response of the porous bed. Both cameras permit continuous photography. This was necessary in these experiments because piston impact of the bed could not be precisely timed, mostly due to variability in the action time of the ignitor for the propelling charge. Rewrite on camera films was prevented by controlling the duration of the xenon flash through the amount of capacitance. In addition, any violent reaction would result in breakage of the nearby turning mirror, which was used to prevent direct fragment impact on the camera port window of the firing chamber.

In some early PDC experiments with Lexan tubes, high-speed photography was used for obtaining compaction data from the motion of thin transparent disks that were packed in the tube between bed increments.[10,11] Disk position was made visible by backlighting the entire tube with a linear flash lamp (General Electric PXA44) attached to the same electronic flash circuit discussed previously. This same technique was used in making compaction measurements with the CGC apparatus.[10,11] In some later PDC experiments, flash radiography was utilized for compaction measurements, as discussed below. Strain gauges were sometimes circumferentially mounted on the outside of the tube to indicate interior pressure.[11] Instrumentation that required a mounting hole in the Lexan tube wall was seldom used in order to avoid weakening the already low confinement. An exception to this was one experiment in which a NaCl window was mounted flush with the inner wall of the tube. This window was required for transmitting infrared (IR) emissions from a compacting/reacting bed of ball propellant; two IR detectors for measuring different frequencies were used to provide a relative temperature.[14]

Flash radiography was used for compaction measurements in Lexan and thin-wall aluminum tubes, both of which could be penetrated by the x-rays from the 150-kV sources in a Hewlett-Packard model 730 system. The technique, which is described in Reference 46, required some small metallic objects (wires, lead pellets, or foil disks) within the porous bed that absorbed the x-rays and thereby served as tracers. When comparing radiographs taken before and during the experiment, the reduced separation of tracers provided a measure of compaction. When comparing radiographs taken at different times during the experiment, the displacement of the tracers provided a measure of both particle and front velocity. As with the transparent disk technique, the particle velocity could be obtained for each tracer between the piston and the compaction front; measurements near the front were those used in jump condition calculations for pressure and extent of compaction. This is in contrast to steel tube experiments, where particle velocities were obtained from photography of scribe lines on the piston as it passed through the barrel extender. It was assumed that these measurements of piston velocity after bed impact provided the location of the end of the piston in the tube as well as the particle velocity behind the compaction front. This assumption was appropriate except for high velocity impact of Lexan pistons, which continuously deformed.

Many of the reported compaction data were obtained from flash radiographs of the intermediate confinement arrangement shown in Figure 2b.[46] The reinforced aluminum tube was designed for four x-ray exposures of the core of the bed during the experiment. Four exposures result in three sets of particle and front velocity measurements. In those experiments, the radiograms were uniformly separated in time, with the last radiogram occurring as the compaction front was near the end of the bed. The arrangement in Figure 2c, which was used just once, permitted two x-ray exposures in conjunction with piezoelectric transducer (PCB 109A02) measurements of inner wall pressure. Some compaction measurements, primarily front velocity, were obtained with microwave interferometry, pin probes, and pressure transducers with the steel tube arrangement in Figure 2d.

Steel tubes are not suitable for high-speed photography and flash radiography without installing large windows, which would weaken the high confinement. To obtain nonintrusive instrumentation for the steel tubes, the microwave interferometer (MI), which is discussed below, was developed and became available for the final experiments. Small holes for mounting instrumentation were drilled into the tube walls without seriously weakening them. Ionization probes (Dynasen, Inc. model CA-1040) and/or self-shorting probes (Dynasen, Inc. model CA-1042) were mounted every 12.7 mm through the tube wall with their sensing ends flush with the inner wall. The self-shorting probes were used for detecting compaction fronts and weakly reactive compressive waves. Up to 10 probes could be connected to a pin switch circuit that generated a coded pulse for display on an oscillocope as each probe responded.[47] In some experiments, measurements of pressure on the inner tube wall were made with several flush-mounted piezoelectric transducers (PCB 109A02), with an upper limit of 0.86 GPa.

The MI was used as a nonintrusive, continuous monitor of the end of the piston after bed impact and the various reflecting wave fronts within the porous bed.[43] As shown in Figure 1, the circular waveguide for the interferometer passed through an opening in the closure end plate and directly mated with the tube. That end of the tube was packed with a specified density of Teflon 7C powder (one of the inert powders used in compaction measurements) to provide a dielectric match between the air in the waveguide and the far end of the porous bed. Through this interface, a continuous frequency (9.0000 GHz) microwave signal is transmitted to the porous bed, where it is both reflected and attenuated. The microwaves reflect from dielectric discontinuities associated with ionization in a reaction zone, the compaction front, and the piston face. The Doppler shifted signal from the moving reflector is mixed with a portion of the original signal to produce a “beat fringe” output. For the most downstream reflector in the bed, which is a compaction/reaction front, a beat occurs every time the front moves one half of the microwave wavelength in the original bed packing. When examining the quadrature output signals for only peaks and valleys, the resolution for locating the first front is actually an eighth of a wavelength, or about 3 mm for the materials that were investigated. The beats from reflectors behind the compaction/reaction front can be analyzed with more difficulty.[43] The MI data were invaluable for locating the downstream front as well as qualitatively outlining the extent of reaction at the front.

The signals from strain gauges, probes, transducers, IR detectors, and MI were recorded on oscilloscopes that were triggered when the piston impacted the bed. Two strips of 3.2-mm-wide copper tape (used for repairing circuit boards) were mounted on the thin plastic disk that covered the end of the bed. The copper contacts were connected to a circuit which would generate a voltage rise when the contacts were shorted through the face of the impacting piston. Lexan pistons had aluminum foil bonded to their impacting end for closing the switch. Early experiments had a trigger pin, just like the one for starting the xenon flash, located just above the end of the bed; time of bed impact had to be estimated knowing the piston velocity. In all of the reported data, time, t, is relative to the piston impacting the bed. Distance, x, is relative to the impacted end of the bed.

Porous Bed Materials and Packing

Dynamic loading studies have been conducted on a variety of materials that are normally produced as grains or were cut into grains. Table I provides for each material the TMD or solid density and the grain dimensions. These grains were packed at uniform density into cylindrically confined beds whose %TMD (volume percent occupied by solid) ranged from 44.2% to 85%.

Some inert materials (Teflon 7C, melamine, and sucrose) were investigated in order to avoid any influence of reaction and to develop experimental techniques. Of the inerts, melamine was primarily used in the development of PDC experiments as a simulant for the two crystalline explosive powders listed in Table I. Of those, HMX was of interest because it is a major ingredient in high-energy propellants. The fine (Class 5, previously Class E) material was the same as that used in DDT experiments at this Center.[4] The coarse HMX used in DDT[4] and shock-to-detonation transition (SDT)[48] experiments at this Center was a sieve cut of larger particles from the Class 4 (previously Class D) material used in the PDC experiments. In addition to experiments at this Center, porous HMX beds (with different particle sizes than used at this Center) have been studied in a dynamic loading experiment[49] by McAfee and co-workers and in a modified wedge test by Dick.[50] The other crystalline explosive powder investigated was tetryl in order to compare PDC data with the only extensive shock loading experiments on a porous explosive, which had been conducted by Lindstrom on coarse tetryl.[34] The same coarse tetryl has been used in PDC, DDT[4] and SDT[48] experiments at this Center. Two plastic-bonded explosives (PBXs) of relatively simple composition (primarily RDX and inert binder) were studied to observe the effect of an inert binder on compressive reaction.[11,15] The same 2-mm cubes of the two PBXs were used in SDT experiments at this Center.[51]

Table I. Description of Porous Bed Materials

Material/Ingredients[a]	TMD[b] (g/cm^3)	Average Particle Size (mm)
Melamine	1.573	0.046-0.056
Crystalline explosives		
Tetryl, coarse	1.73	0.470
HMX, Class D	1.90	0.870
HMX, #20 sieve cut of Class D	1.90	0.925
HMX, Class E	1.90	0.015
Plastic bonded explosives		
PBXW-108(E), RDX/HTPB	1.555	2.17 (cubes)
PBXW-109(E), RDX/Al/HTPB	1.655	2.17 (cubes)
Ball propellants		
Fluid A, NC	1.65	0.034 (spherical)
WC 140, NC	1.65	0.411 (mostly spherical)
TS 3660, NC/12% NG	1.64	0.714 (spherical)
TS 3659, NC/21.6% NG	1.64	0.434 (spherical)
WC 231, NC/~25% NG	1.64	0.79 dia. x 0.23 thick disks
High-energy propellants, Al/AP/HMX/energetic binder/NG		
HEP "X"	1.88	0.5 x 1.6 x 25 rough shreds
ABL 2523 (HEP "Y")	1.895	1.3 dia. x 1.3 long cylinders
RS 075 (HEP "Z")	1.84	0.8 x 2.5 x 1.6 short shreds 6.4 long shreds

[a] Al = aluminum AP = ammonium perchlorate
NC = nitrocellulose HMX = cyclotetramethylenetetranitramine
NG = nitroglycerin RDX = cyclotrimethylenetrinitramine
HTPB = hydroxyterminated polybutadiene (inert binder)

[b] Theoretical maximum density

Ball propellants were extensively studied as simple models of damaged high-energy propellants. Some of the ball propellants were useful for guiding the development of numerical models because they consisted of only one or two ingredients, had spherical particles of uniform size, and deformed plastically in a predictable manner. Their deformation was more like the high-energy propellants rather than the fracturing of HMX, which produces an unknown distribution of smaller particles. Also, some of the ball propellants were sufficiently reactive to undergo DDT in steel tube experiments conducted at this Center by Bernecker.[48,52,53] TS 3659 was nearly ideal in these respects. A series of well-instrumented PDC experiments on TS 3659 and WC 140 was modeled by a number of investigators, who shared their predictions at a JANNAF sponsored workshop.[38]

The three high-energy propellants listed in Table I were cross-linked, double-base compositions containing aluminum, ammonium perchlorate, HMX, and an energetic binder that was plasticized with nitroglycerin (NG). The mechanical properties of the propellants differed considerably; ABL 2523 was much stiffer than HEP “X” and

RS 075. ABL 2523 is a casting powder in the form of cylindrical granules (1.3 mm diameter by 1.3 mm long) that are already suitable for packing in a porous bed. The HEP “X” and RS 075 were shredded from large pieces of cast propellant. The HEP “X” shreds were approximately rectangular (0.5 mm by 1.6 mm by 25 mm) but had rough surfaces and irregular shapes. The HEP “X” shreds were stored for about 8 years before these experiments; shreds from the same batch were previously used in DDT experiments.[54] Large pieces of RS 075 were turned on a lathe to produce long, fairly uniform (0.8 mm thick by 2.5 mm wide) strands that were cut to lengths of 1.6 or 6.4 mm with razor blades; the two lengths are referred to as short and long shreds respectively. RS 075 was designated as HEP “Z” in References 15 and 33, and ABL 2523 was designated as HEP “Y” in Reference 15.

Porous beds were normally packed by weighing the amount of material for a prescribed increment height, pouring it into the tube, and then hand pressing it to stops with a Teflon-tipped brass rod. This provided uniform density for the entire bed, which was up to 150 mm long. Increments of 12.7 mm were usually used; for flash radiography measurements, a small metallic tracer was placed between each increment, which was reduced in length to 6.4 mm to improve spatial resolution of density gradients. Hand packing of stiff materials, such as crystalline explosives and ball propellants, generally resulted in only the one stable bed density. Since >4 MPa was required to pack coarse tetryl to 75.1% TMD, as had been investigated by Lindstrom,[34] those beds were pressed remotely in a frame with a hydraulic jack.

EXPERIMENTAL RESULTS

Inerts

Inert porous beds, primarily of melamine, were used to develop experimental techniques without any complications from bed reaction. The summary of melamine experiments in Table II is much like the following summaries for energetic materials except for the absence of reaction data. The initial conditions listed in Table II for each experiment include: initial bed packing in terms of percent volume occupied by the solid (%TMD_o), bed length (L), type of tube which confined the bed, and piston velocity just before bed impact (v_p). Of the results listed in Table II, only the particle velocity (u) and compaction front velocity (U) are experimentally measured. These parameters are used in jump condition calculations for extent of compaction,

$$\%TMD = \%TMD_o/(1-u/U) \tag{1}$$

and axial compaction pressure or average bed pressure,

$$p(MPa) = p_o + \%TMD_o{*}TMD{*}U{*}u{*}10^{-5}, \tag{2}$$

where the initial pressure (p_o) is 0.1 MPa (atmospheric pressure) and both u and U are in units of m/s. Direct measurements of %TMD were often made in Lexan and aluminum tubes and agreed with jump condition calculations within ±2%. The jump calculations for %TMD are shown in order to be consistent with the pressure calculations. Compaction pressures, especially in reporting quasi-static data, often were reported in terms of an intragranular or average solid stress, τ_i, instead of an average bed stress, p. The two are related by the bed fraction occupied by solid according to

$$\tau_i = 100p/\%TMD. \tag{3}$$

The first PDC experiment (Shot PDC-2) had 60% TMD Teflon 7C packed in a Lexan tube with transparent disks every 25.4 mm. The framing camera film of the backlit tube showed that the ~270 m/s impact so strongly compacted the bed that the tube began to expand immediately and had cracked open before the compaction front reached the end of the 137-mm-long bed. A similar experiment was conducted on 65% TMD melamine (Shot PDC-3) at a somewhat slower piston velocity of 190 m/s and the tube did not crack. Thus, the low confinement of Lexan tubes limited piston impacts to ~200 m/s if tube integrity was required for several hundred microseconds. In these and several subsequent experiments, it was also recognized that the transparent disk technique would not be as successful as it was at the lower compaction pressures in the CGC experiments. The disks were no longer visible after a SCW reached them, and the disks also perturbed the growth of compressive reaction. Because of these deficiencies with transparent disks, flash radiography was used for further compaction measurements.

Calculations of u and %TMD from flash radiographic measurements, as well as those obtained by the transparent disk technique, are sensitive to small changes in tube diameter. For beds packed in Lexan tubes, the higher pressures in the PDC experiments, relative to the earlier IDC and CGC experiments, required correction of compaction data for tube expansion.[10,11] The melamine data in Table II show both uncorrected and corrected compaction data for three Lexan tube experiments (Shots PDC-3, -16, -17). In these experiments tube expansion is calculated assuming that the inner wall pressure (p_w) is the same as p; that is, the bed is in a state of hydrostatic stress. This correction reduces the extent of compaction from 94.0 to 84.7% TMD for the highest compaction pressure, ~75 MPa in Shot PDC-16. Subsequent radiographic measurements for dynamic compaction (Shots PDC-41A,B) were made in the reinforced, thin-wall aluminum tube shown in Figure 2b to avoid a large and uncertain correction for tube expansion. Multiple radiographic measurements, such as those for Shot PDC-41B, are tabulated in the order of time from bed impact.

Table II. Summary of Melamine Experiments

	INITIAL CONDITIONS				RESULTS				
SHOT	$\%TMD_o$	L (mm)	TUBE+	v_p^* (m/s)	u* (m/s)	U (m/s)	%TMD	p (MPa)	INSTRUMENTATION**
PDC-41A		133	Alum.	~70	52	293	79.0	15.7	
PDC-17		146	Lexan	122	96	384	86.6	37.8	
						‡	82.3	36.8	Flash X-rays
PDC-16		146	Lexan	~170	153	495	94.0	77.5	
						‡	84.7	73.4	
PDC-3		137	Lexan	190	148	480	93.9	72.7	Streak photography of trans-
						‡	85.1	69.1	parent disk in bed every 25.4 mm
					157	539	91.7	86.6	
PDC-41B	65.0	133	Alum.	~170	155	534	91.5	84.7	Flash X-rays
					140	498	90.4	71.4	
M-19		89	Steel	204++	187	619	93.1	118.4	Self shorting probes
M-26		305	Steel	206	165	518	95.4	87.4	---
M-29		72	Steel	212	160	521	93.8	85.3	Self shorting probes
					204	614	97.3	128.1	
M-34		146	Steel	206++	189	585	96.0	113.1	Self shorting probes, three
					173	556	94.3	98.4	pressure transducers
					152	516	92.1	80.3	
PDC-74	85.0	86	Steel	217++	191	1250	100.3	319	Self Shorting probes and pressure transducer in closure plate

See Glossary for parameter definitions

\+ Lexan = thick-wall Lexan tube in Figure 2a
Alum. = Supported thin-wall aluminum tube in Figure 2b
Steel = thick-wall steel tube in Figure 2d

* Usually measured by streak photography of piston. Where '~' precedes number for v_p, no streak record was obtained. When flash X-rays were obtained, reported values for u are by that technique

** All M- series shots had microwave interferometry in addition to other instrumentation

‡ Calculations for %TMD and p corrected for tube expansion by assuming the wall pressure equalled p

++ Aluminum Piston

The quasi-static compaction data for melamine[17] are plotted in Figure 3 together with the dynamic data listed in Table II. The radiographic data from intermediate confinement Shots PDC-41A,B agree quite well with the quasi-static data. When expansion of the Lexan tubes was not corrected for, the dynamic data for %TMD were high relative to quasi-static measurements at the same pressures. The dynamic data were overcorrected when accounting for tube expansion by assuming $p_w = p$. In some Lexan tube experiments on materials other than melamine, tube expansion was directly measured with circumferentially mounted strain gauges and found to less than that from assuming $p_w = p$. In a steel tube experiment on melamine (Shot M-34), which is discussed below, transducer measurements of p_w were less than p. The prediction of Lexan tube expansion during compaction also applies to the analysis of the early stages of DDT in those same tubes.

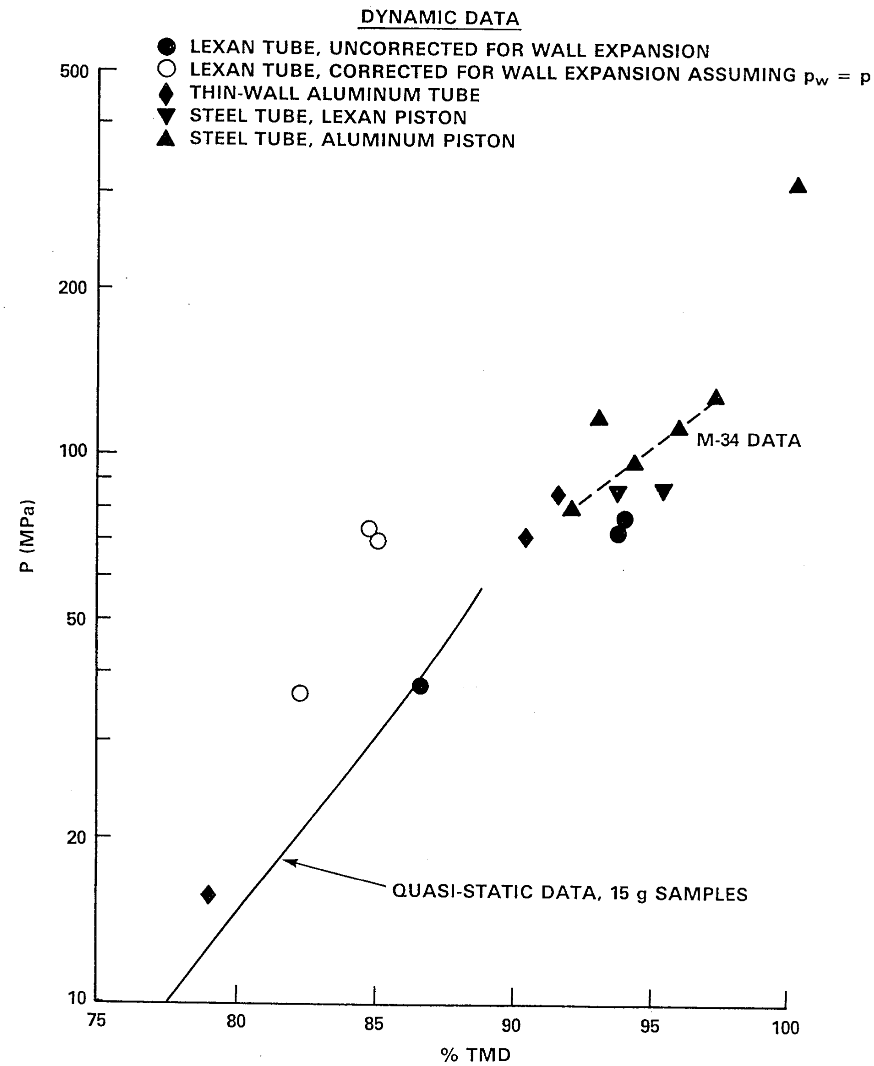

Figure 3. Compaction Data for Melamine Powder

Melamine beds were used during the development and verification of the MI technique in steel tube experiments. While intermediate confinement was sufficient for 1-D measurements of dynamic compaction, the high confinement of steel tubes was necessary for 1-D measurements during the rapid pressure build-up in reacting energetic materials. Melamine was hand loaded at 65% TMD in steel tubes and impacted by Lexan pistons in Shots M-26 and -29 and by aluminum pistons in Shots M-19 and -34. The plot of dynamic and quasi-static compaction data in Figure 3 shows somewhat greater compaction for the same pressure with Lexan versus aluminum pistons in steel tube experiments. The Lexan driver data are similar to the uncorrected Lexan tube data, which also had a Lexan driver. Thus, there may be some effect of the driver on the compaction measurements. One melamine bed was packed at 85% TMD in a steel tube, which is a much higher density than possible by hand, in order to certify a remote hydraulic press for loading 75.1% TMD coarse tetryl. As shown in Figure 3, all the steel tube experiments for melamine achieved greater %TMDs than the maximum 89% TMD obtained quasi-statically. Since higher %TMDs should require at least a linear extrapolation in stress, it appears that melamine is easier to compact dynamically than quasi-statically above ~90% TMD.

In the final melamine experiment, Shot M-34, the steel tube was instrumented with self-shorting probes (every 12.7 mm), MI, and three pressure transducers. The transducers were used to confirm MI data and to obtain a better understanding of pressure transducer traces from the ball propellant experiments in References 12 through 14. In previous experiments, self-shorting probes did not always respond promptly as the compaction front passed their location, and so were not viewed as adequate verification of MI data. Before installing the probes in Shot M-34, they were manually pushed against a plate to short-circuit their sensing tip, while monitored with a resistance meter. The sensing tip returned to an open-circuit condition as soon as the probe was released but required less force to short-circuit when the probe was pushed into the plate again. Also, there was much less variation in the force required to short-circuit different probes after conducting the above procedure. Some improvement in the uniformity of the response of these probes was noted in Shot M-34.

The distance-time data and pressure transducer traces from Shot M-34 are plotted in Figures 4a and 4b, respectively. In Figure 4a, the path of the compaction front as determined from microwave data was verified by the responses of the self-shorting probes and pressure transducers. Whereas constant U and u are usually reported, both velocities had a small (but linear) decline with time. The equations for U and u are listed on Figure 4a, and calculated values from those equations are listed in Table II for the beginning of the bed and when the compaction front reaches each pressure transducer. The jump condition calculations for %TMD and p are plotted in Figure 3. The dashed line through those data points has a significantly lower slope than the quasi-static data, indicating the relative ease for compaction at high TMDs. The extent of compaction was especially high (97.3% TMD) at the impacted end of the bed, which experienced the highest strain rate because the compaction wave has just begun to diffuse. The high calculated %TMD (Equation 1) at the impacted end of the bed should be valid since U was well defined over the entire bed length and the most accurate value of u would be when the piston is near the compaction front.

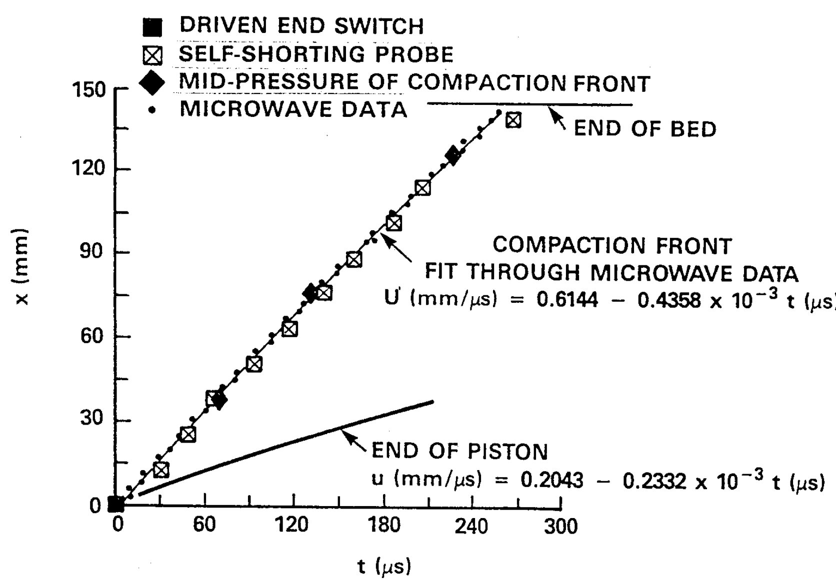

a. Summary of distance-time data

Figure 4. Data from a 206-m/s Impact of 65.0% TMD Melamine in a Steel Tube (Shot M-34)

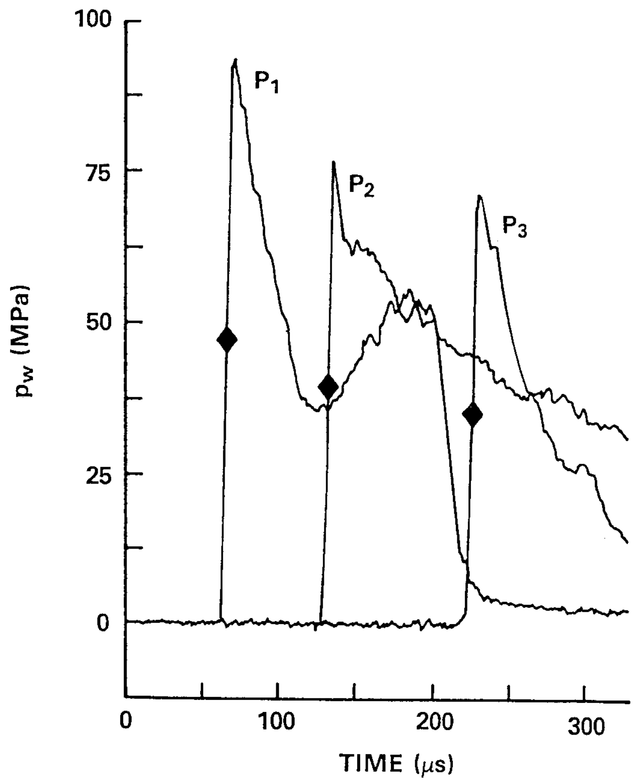

b. Inner wall pressures at 38.2 mm (P_1), 76.4 mm (P_2), and 127.0 mm (P_3)

Figure 4. Data from a 206-m/s Impact of 65.0% TMD Melamine in a Steel Tube (Shot M-34) (Continued)

The transducer traces in Figure 4b show that the gradual slowing of the piston causes the peak pressures at the inner wall to fall from 93.7 MPa at 38.2 mm (P_1) to 77.1 MPa at 76.4 mm (P_2) to 72.0 MPa at 127.0 mm (P_3). The ratios of p_w to p varied from 78% to 89%. There was a relatively rapid falloff in pressure as soon as the peak was obtained at each transducer; this falloff was partly due to the rarefaction from the slowing piston. Also, as soon as the compacted bed began to slide past the slightly recessed transducers, they may no longer accurately record radial stress. The P_1 trace is particularly interesting because the pressure rapidly declined just after the peak and then gradually increased until the piston reached the transducer location at ~200 µs. It is speculated that the actual radial stress monotonically declined between the peak at 74 µs and the arrival of the piston at ~200 µs. A monotonic decline was obtained by Kooker when modeling this experiment (Figure 30 of Reference 55).

Explosives

Much of the PDC data on HMX has been reported,[11,15,31,33] except for the recent experiments with MI. The HMX experiments are listed in Table III, where Δt is the time between bed impact and detection of reaction and x_D is the distance to detonation. Quasi-static and dynamic compaction data from this Center are compared in Figure 5 for several particle sizes. Most of the dynamic data are from intermediate confinement experiments; data[15,31] from Lexan tubes without strain gauge instrumentation for measuring tube expansion are not plotted. Dynamic data[15,33] from steel tubes are also not plotted because reaction probably had an immediate effect in these experiments with typically high piston velocities. The quasi-static data in Figure 5 for the various sieved fractions show that the finer particle sizes require more stress to compact. Although Class D HMX has an average particle size of 870 μm (slightly smaller than the 925 μm particles in the #20 sieve cut), Class D is somewhat easier to compact, probably because its wide particle size distribution improves packing efficiency of the original particles and those fractured during the compaction process. Although not shown, there is a wide variation in the quasi-static compaction behavior of Class D HMX, and some Class D beds were easier to compact than the #20 sieve cut. (The variation in Class D HMX compaction may result from significant differences in particle size distribution of the samples, even though obtained from the same container, given the wide particle size distribution of the material.) If Class E HMX (average particle size of 15 μm) had been compacted quasi-statically, the plot of τ_i versus %TMD would presumably be to the left of the data for 85 μm HMX. Assuming this is the case, then compaction of both fine and coarse HMX is somewhat easier dynamically than quasi-statically. However, as just mentioned, there is a variation in the quasi-static compaction behavior of Class D, and the dynamic data tend toward quasi-static experiment HMX-24,[25] which was the easiest bed to compact.

The dynamic data in Figure 5 for Class D HMX are consistent except for an unusually high %TMD calculated near the impacted end of the bed in Shot M-21. The compaction measurements from the first radiograph in Shots M-20, M-21, and M-22 were 91.5%, 91.0%, and 94.5% TMD, respectively, all of which are low relative to the jump calculations shown in Table III. These low densities and the initially higher amplitude return signals from the MI in Shots M-21 and M-22 indicate that there was some early reaction which quenched. That quenching resulted in a lower value of U between the first two radiographs in Shot M-21; a lower U increased %TMD and reduced p in the calculated values listed in Table III. It is interesting to note that growth of compressive reaction was not observed in the intermediate confinement experiments M-21 and M-22, which had slightly higher piston velocities than Lexan tube Shot PDC-22 and steel tube Shot PDC-70. A similar inhibition of compressive reaction in intermediate confinement also occurred in Class E HMX experiments.

The growth of compressive reaction for Class D HMX in steel tube confinement was recorded by pressure transducers and the MI in PDC Shot M-33. As shown in the distance-time plot in Figure 6a, the 213 m/s Lexan piston impact resulted in a relatively steady compaction front velocity for ~70 μs, followed by an accelerating front, which transited to detonation ~15 μs later at 63 mm. A pressure transducer at 38.3 mm was located near where the front velocity began to accelerate. The pressure-time plot in Figure 6b shows an almost steady rise in pressure that continued beyond the ~900 MPa limit of the transducer. There is no separation on the trace between compaction (p = 100 MPa) and the onset of compressive reaction. A pressure transducer at 89.1 mm responded instantaneously as the detonation wave passed its location. The piston slowed at a linear rate, u(m/s) = 147.59 - 0.45714 t(μs), prior to 65 μs. Following that, the rapid deceleration of the piston just preceded the rise of pressure recorded by the 38.3-mm transducer that began at 70 μs. The 134-m/s particle velocity for the face of the piston that is reported in Table III occurred 30 μs after impact. The 539-m/s compaction front velocity reported in Table III is based on the time between closure of the driven end switch and the recording of the mid-pressure observed for the compaction front by the 38.3-mm transducer. This value of U is comparable to the 553 m/s obtained with the MI, which is discussed below.

In the predetonation zone in Shot M-33, the two pin probes and the pressure transducer responded after the passage of the front according to the MI. If the MI data were shifted in ‘x’ by 5 mm, the front would correlate with the transducer response in the predetonation zone as well as the probe responses in the region of detonation. Most of the shift would occur by ignoring the initially high U just after impact and assuming that U was the steady 553 m/s recorded for most of the predetonation zone. The MI signal from the front just after piston impact did not have an increased amplitude indicative of early reaction, and thus a higher front velocity, as in Shots M-21 and M-22. Also, the MI signal from dynamic compaction just after bed impact could be misinterpreted, partly because that signal for 73% TMD HMX is small. The compaction signal results from the change in relative dielectric constant, which is 1.13 for full compaction of 73% TMD HMX versus 1.82 for full compaction of 65% TMD melamine.[44]

Table III. Summary of HMX Experiments

MATL.	SHOT	%TMD$_o$	L (mm)	TUBE	v_p (m/s)	u (m/s)	U (m/s)	%TMD	p (MPa)	Δt (μs)	COMMENTS
	INITIAL CONDITIONS					RESULTS					
						55	300	88.1	22.8		
	PDC-21		146	Lexan	74	58	304	88.9++	24.4	---	No reaction
						52	280	88.4	20.2		
						76	359	90.6	37.5		
	PDC-25		133	Lexan	102	79	347	92.5++	37.7	394	Weak reaction
						81	364	91.9	40.5		
						80	393	91.7	43.7		
	PDC-54		133	Alum.	---	79	382	92.2	42.1	---	No reaction
						78	369	92.5	40.0		
	M-20		127	Alum.	---	92	418	93.7	53.4	---	Early failure
						92	402	94.7	51.4		
	PDC-22		133	Lexan	125	102	438	95.2	62.1	117	Weak reaction
								87.5**	59.5		
HMX Class D	PDC-70	73.0	178	Steel	~150	~107	447	~96	~66	---	x_D = 114-127 mm
						110	424	98.6	64.8		
	M-21		127	Alum.	---	111	483	94.8	74.5	---	Interferometer
						113	482	95.4	75.6		data indicates
						117	473	97.0	76.9		early reaction
	M-22		127	Alum.	---	116	475	96.6	76.5	---	that dies out
						115	502	94.7	80.2		
	M-33		146	Steel	213	134	539	97.2	100	<70	x_D = 63 mm
	PDC-59		177	Steel	223	144	540	99.5	108	<42	x_D = 39 mm
	PDC-27		133	Lexan	267	161	~775	92.1	173	~21	x_D = 50 mm
	M-23		83	Steel	303+	276	1023	100‡	392	<7	x_D = 14.5 mm
	PDC-69		86	Steel	356	~250	926	100*	321	<18	x_D = 27 mm
HMX #20 Sieve cut of Class D	PDC-63A	60.0	76	Alum.	---	62	211	85.0	15.0	---	No reaction
						64	213	85.8	15.6		
						117	334	92.4	44.6		
	PDC-63B	60.0	76	Alum.	---	118	336	92.5	45.3	---	No reaction
						118	337	92.3	45.4		
						71	178	73.5	10.7		
	PDC-53		133	Alum.	---	75	184	74.6	11.7	---	No reaction
						71	179	73.3	10.8		
						108	255	76.7	23.2		
	PDC-56		133	Alum.	---	103	243	76.6	21.1	---	No reaction
						99	234	76.5	19.5		
HMX Class E	PDC-39	44.2	137	Steel	200	160	360	79.6	48.5	<215	x_D = 81 mm
						180	387	82.7	58.6		
	PDC-58		133	Alum.	202	174	372	83.1	54.5	---	
						167	337	87.6	47.4		
	PDC-46		146	Lexan	216	170	362	83.4	51.8	215	Weak reaction
	PDC-50		146	Lexan	308	252	495	90*	105	52	x_D = 40 mm

+ Aluminum Piston
‡ Assumed %TMD and measured v_p used to calculate u, U, and p
* Assumed %TMD and measured u used in calculations for U and p
++ Calculations for %TMD and p corrected for tube expansion as measured by strain gauges
** Calculations for %TMD and p corrected for tube expansion by assuming wall pressure = p

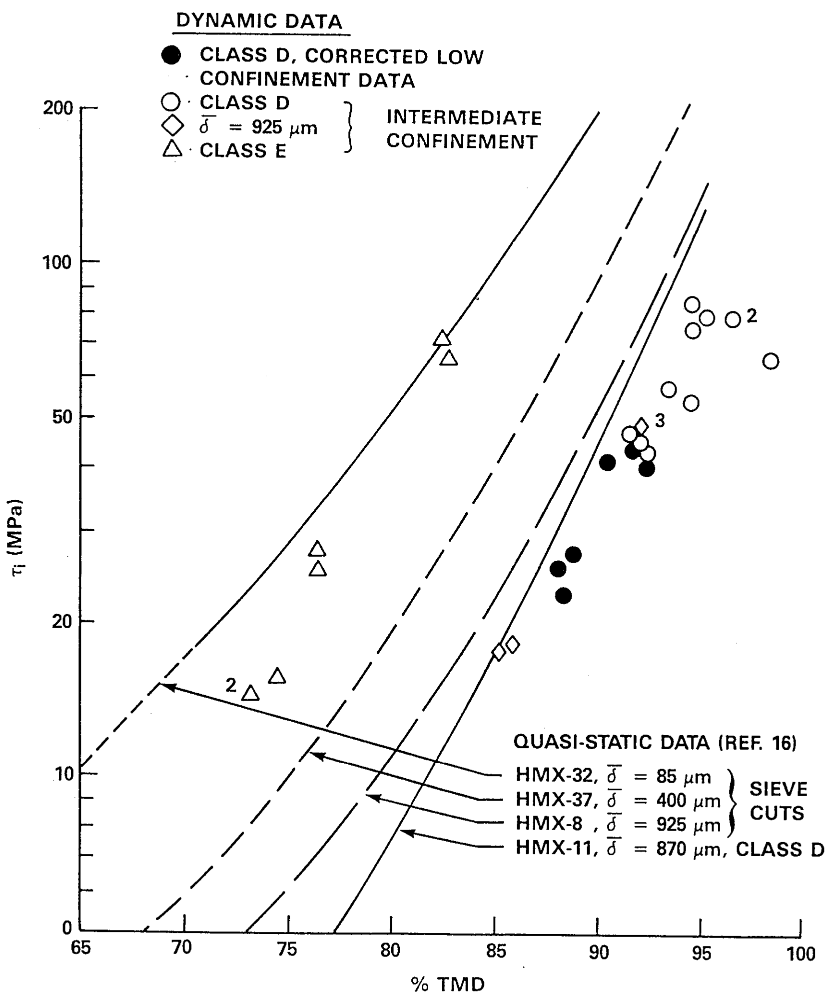

Figure 5. Compaction Data for Various HMX Powders

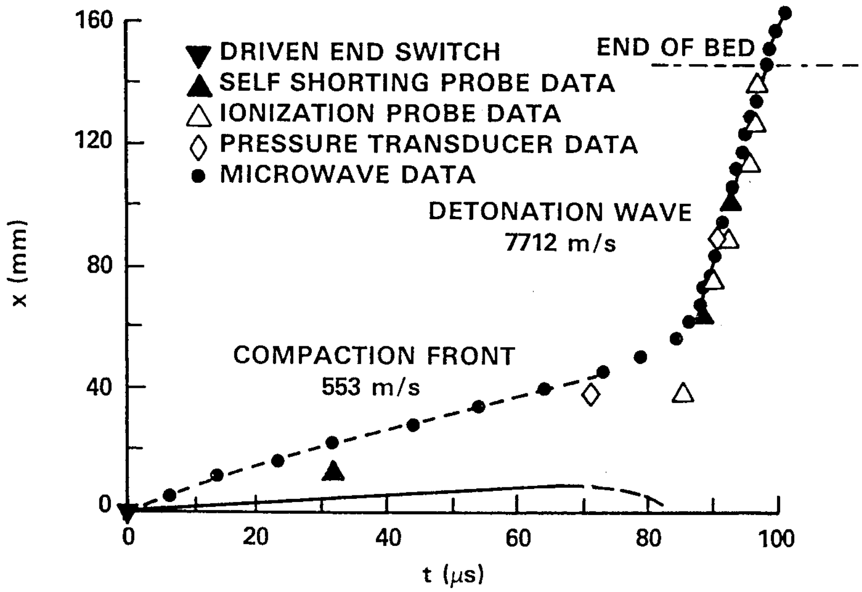

a. Summary of distance-time data

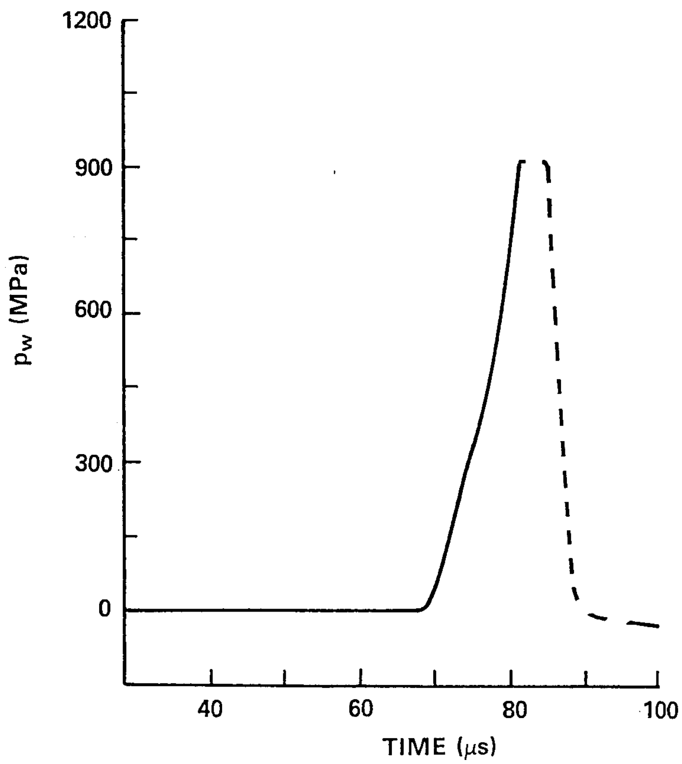

b. Inner wall pressures at 38.3 mm

Figure 6. Data from a 213-m/s Impact of 73.0% TMD Class D HMX in a Steel Tube (Shot M-33)

Coarse tetryl experiments are listed in Table IV. Only Shots PDC-13 and PDC-57, which were hand loaded at 57.8% TMD in Lexan tubes, have been previously reported.[15] In Shot PDC-13, weak luminosity was recorded along much of the bed ~163 μs after passage of the compaction front. This experiment had transparent disks, every 25.4 mm in the bed, that barricaded the spread of the weak luminosity. In Lexan tube Shot PDC-57, the coarse tetryl transited to detonation in 36 mm from a ~290 m/s impact; the missing data in Table IV is due to failure of the electronic flash.

A series of coarse tetryl experiments (Shots PDC-75, -83, -84 and M-32) had aluminum pistons impacting highly confined beds packed to 75.1% TMD in steel tubes. The high confinement approximated a one-dimensional run to detonation in an attempt to extend the wedge test data of Lindstrom[34] to lower shock pressures. The combination of prompt initiation of compressive reaction and the inability to photograph events within the steel tubes permitted no measurements of Δt. The onset of reaction was delayed just long enough in the lowest velocity impact, Shot M-32, for a MI measurement of U; this is the only experiment in this series with direct measurements of both u and U. In higher velocity impacts, the onset of reaction occurred so quickly that it was not possible to determine u from the streak record of scribe lines on the impacting piston. At the highest impact velocity, the piston does not appear to enter the tube, probably because the piston was stopped by the rapid onset and growth of reaction. To obtain bed pressures for the higher velocity impacts, impedance calculations for the impacting aluminum piston and bed were made assuming no porosity remained in the bed. At the two highest impact velocities, the values of p calculated by this technique were in the pressure range of the Hugoniot reported by Lindstrom; therefore, his equation[34] was also used to calculate the shocked state. As shown in Table IV, the Hugoniot calculation of compaction and compression to 107.8% TMD in the highest velocity impact, Shot PDC-84, is lower than the 114.5% TMD calculated for the somewhat lower velocity impact in Shot PDC-83. This does not seem reasonable and probably resulted from the effects of reaction on the Hugoniot measurements.

Experiments on PBXW-108(E) and PBXW-109(E) (now PBXN-109) are also listed in Table IV. The flash radiographic measurements of compaction showed that both PBXs were easily compacted.[11] Even at the lowest impact pressure (~20 MPa) that was examined, the beds were compacted to TMD. Although all the data except for Shot PDC-42 were obtained in Lexan tubes, reasonable corrections for tube expansion were made based on strain gauge measurements. Both PBXs were also relatively insensitive to compressive reaction.[15] The only observations of compressive reaction in the Lexan tube experiments were faint traces of luminosity, except that no luminosity was observed for the highest velocity impact on PBXW-109(E) in Shot PDC-31. With essentially the same impact velocity as Shot PDC-31, the aluminum tube in Shot PDC-42 ruptured. Referring to Figure 2b, the sections of thin-wall tube between the steel supports were sheared away. The level of reaction responsible for tube failure is not known. Even the weak reaction observed in Lexan tubes may have been sufficient for failure of the aluminum tube, since it was already well stressed from the high compaction pressure (119 MPa) and its thin wall lacks the inertia of the much thicker wall in the Lexan tube.

Ball Propellants

Experiments on a variety of ball propellants, all impacted with Lexan pistons, are listed in Table V. Except for Shot PDC-72 on Fluid A, these experiments were previously reported. Low confinement (Lexan tube) compaction data for Fluid A, WC 140, TS 3660 and WC 231 from CGC and PDC experiments, up to and including Shot PDC-24, were included in Reference 11; and many of those experiments were summarized in Reference 10. The Lexan tube data, which are plotted together in Figure 14 of Reference 11, were obtained over only the beginning of the compaction range. Large and uncertain corrections for expansion of the Lexan tubes would have been required at the higher bed pressures necessary for more extensive compaction. Dynamic compaction data with minimal influence from tube expansion were obtained over most of the compaction range (pour density to >93% TMD) from intermediate and high confinement experiments on WC 140[13] and TS 3659[12.] In addition, there was a single intermediate confinement experiment on Fluid A, Shot PDC-72. Experimental data for WC 140 and TS 3659, both consisting of mostly spherical particles with sizes somewhat greater than 400 µm, are compared to show the effect of NG content, 0 and 21.6%, respectively (Table I). Fluid A and WC 140 data are compared to show the effect of particle size, 34 and 411 µm, respectively, for NC powders (0 %NG).

Table IV. Summary of Tetryl and PBX Experiments

MATL.	SHOT	INITIAL CONDITIONS %TMD$_o$	L (mm)	TUBE	v_p (m/s)	RESULTS u (m/s)	U (m/s)	%TMD	p (MPa)	Δt (µs)	COMMENTS
Coarse Tetryl	M-32	75.1	86	Steel	188+	176	677	101.5	155	<40	x_D = 37.3 mm
						177	711	100‡	164		
	PDC-75		92		258+	238	956	100‡	296	<12	x_D = 18.4 mm
	PDC-83		32		309+	281	1129	100‡	412	---	x_D = 15.8 mm
						288	836	114.5#	312		
	PDC-84		25		350+	315	1265	100‡	518	---	x_D = 12.0 mm
						320	1057	107.8#	440		
	PDC-13	57.8	137	Lexan	190	149	38.0	95.1	56.7	163	Weak reaction
	PDC-57		133		~290	---	---	---	---	---	x_D = 36.0 mm
PBXW-108(E)	PDC-28	75.0	145	Lexan	72	66	227	100.2	19.1	---	No reaction
						62	229	98.9*	17.6		
						70	258	96.5	19.7		
	PDC-29				134	112	375	101.1	47.6	---	No reaction
						114	386	100.6*	49.9		
						109	363	101.3	44.8		
	PDC-30				260	151	457	100.8	76.2	167	Weak reaction
						154	426	105.7*	72.5		
						162	440	106.8	78.7		
PBXW-109(E)	PDC-20	75.0	133	Lexan	75	61	276	94.3	20.8	---	No reaction
						57	247	95.6*	17.4		
						57	238	96.6	16.8		
	PDC-23		121	Lexan	128	102	364	98.3	44.8	<361	Weak reaction
						109	348	103.0*	45.8		
						108	336	104.2	43.8		
	PDC-26		121	Lexan	178	117	404	96.2	56.0	<258	Weak reacton
						137	418	101.6*	67.9		
						146	424	104.2	73.4		
	PDC-31		121	Lexan	280	175	477	103.8	96.9	---	Reaction not luminous
								*			
						169	449	105.4	88.1		
	PDC-42		121	Alum.	~270	159	602	101.9	118.9	<156	Tube ruptured

+ Aluminum Piston

‡ Assumed %TMD and measured v_p used in calculations for u, U, and p

Lindstrom's Hugoniot for 75.1% TMD tetryl used to calculate u, U, %TMD and p

* Calculations for %TMD and p corrected for tube expansion as measured by strain gauges

Table V. Summary of Ball Powder Experiments

MATL.	SHOT	%TMD$_o$	L (mm)	TUBE	v_p (m/s)	u (m/s)	U (m/s)	%TMD	p (MPa)	Δt (μs)	COMMENTS
	INITIAL CONDITIONS					RESULTS					
	CGC-18	60.6	140	Lexan	---	~24	260	66.2+	6.3	---	
	CGC-19	60.6	140	Lexan	---	~32	320	66.4+	10.3	---	
						62	346	68.2	20.2		
	PDC-19	57.6	146	Lexan	~70	60	324	68.9+	18.3	---	
FLUID A						52	267	70.2	13.2		
						109	413	75.8	42.2		Non-lum. reaction
	PDC-24	57.6	146	Lexan	129	109	410	76.0++	41.9	518	follows far end
						112	425	75.7	44.6		reflection of CF
						118	436	78.9	49.0		
	PDC-72	57.6	133	Alum.	~160	116	423	79.3	46.7	---	Tube intact
						110	423	77.8	44.3		
	CGC-12	60.0	140	Lexan	---	30	380	64.1+	11.3	---	
	CGC-13	60.0	140	Lexan	---	50	460	65.2+	22.5	---	
	CGC-14	60.0	140	Lexan	---	45	400	66.0+	17.7	---	
						57	455	69.0	25.9		
	PDC-62A	60.4	101	Alum.	~75	56	448	69.0	25.1	---	Tube intact
						54	453	68.5	24.5		
						100	503	75.5	50.3		
WC 140	PDC-62B	60.5	101	Alum.	~161	102	548	74.3	55.9	---	Tube intact
						95	512	74.3	48.6		
						156	594	82.0	92.6		
	PDC-64	60.5	126	Alum.	~200	146	552	82.2	80.5	---	Tube ruptured
						145	559	81.7	81.0		
	PDC-71	60.5	191	Steel	180	134	558	79.8	74.7	<200	growth @152 mm
	M-30	60.5	146	Steel	210	161	563	84.7	90.6	119	Late reaction
	M-31	60.5	146	Steel	300	204	574	93.9	117.	~133	Late reaction
TS 3660	CGC-16	57.6	140	Lexan	---	32	343	62.6+	10.4	---	
	CGC-17	57.6	140	Lexan	---	50	369	65.0+	17.3	---	
	PDC-76	60.2	146	Lexan	~150	---	---	---	---	---	Tube intact
	PDC-77	60.2	146	Lexan	~200	---	---	---	---	---	Tubes ruptured but no luminous
	PDC-78	60.2	146	Lexan	291	207	---	---	---	83	reaction seen
TS 3659	PDC-80	60.2	102	Alum.*	160	127	494	81.0	62.0	100	Tube ruptured
	PDC-81	60.1	147	Steel	237	192	534	93.9	101	84	Tube intact
	PDC-82	60.1	147	Steel	300	216	557	98.2	119	<80	Tube intact
	CGC-23	49.4	292		---	73	251	68.2+	14.8	1090	Weak Reaction
	CGC-22	50.0	140		---	85	277	70.2+	19.2	679	Weak Reaction
	PDC-9	49.4	137		110	95	300	71.3++	23.0	---	
WC 231	PDC-12	49.4	137	Lexan	120	104	313	71.3+	26.0	511	Weak Reaction
	PDC-4	50.0	137		~190	---	---	---	---	---	Vigorous Reaction
	PDC-73	49.4	133		220	183	405	90.1	60.1	119	Vigorous Reaction
	PDC-60	49.4	133		380	310	669	92.1	168	31	x_D = 84 mm

*Arrangement shown in Figure 2c
+Calculations for %TMD and p corrected for tube expansion by assuming wall pressure = p
++Calculations for %TMD and p corrected for tube expansion as measured by strain gauges

Dynamic compaction data from only intermediate and high confinement experiments are shown in Figure 7 to avoid uncertainties associated with Lexan tube expansion. For comparison with the dynamic data, fits to quasi-static data for Fluid A, WC 140, TS 3659, and WC 231 are also shown. These fits were obtained from the lattice compaction model[29] using the approach that the particles are packed as a mixture of simple and face-centered cubic lattices. One of the two fit parameters required is the fraction of simple cubic lattices (f_{sc}), which is determined from the $\%TMD_o$ using Equation 14 of Reference 29. The other fit parameter is the average yield stress (p_y) over the contact areas between particles, which is adjusted until the fit matches the quasi-static data. The fit parameters are listed in Table VI for the quasi-static compaction of each ball propellant plotted in Figure 7; more fit parameters are listed in Table 4 of Reference 29. For WC 140, the value of f_{sc} corresponds to the 60.5% TMD_o of the PDC experiments, whereas the quasi-static measurements were obtained on beds packed at 57.8% TMD. A fit through the actual quasi-static measurements and the slightly shifted fit for 60.5% TMD are shown together in Figure 2a of Reference 13.

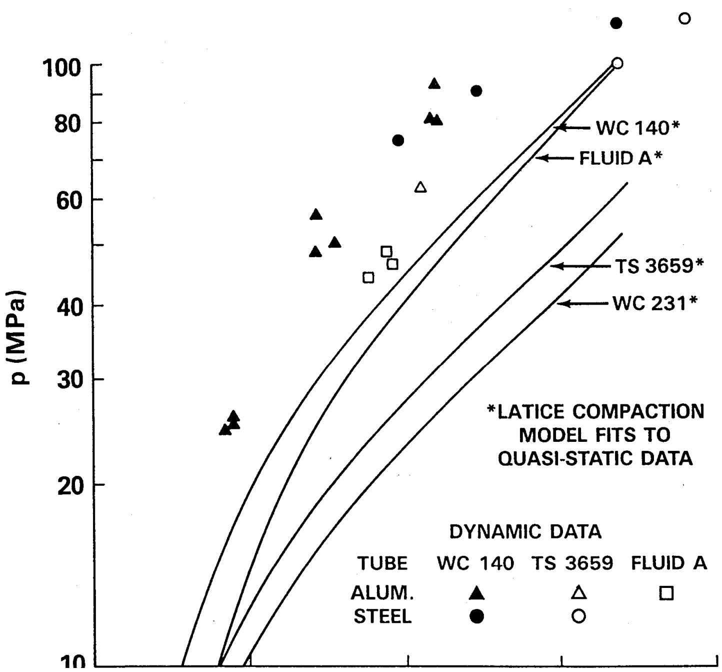

Figure 7. Compaction Data for Various Ball Propellants

Table VI. Parameters for Mixed Lattice of Compaction in Ball Propellants

Material	f_{sc}	p_y (MPa)
Fluid A	0.422	160
WC 140	0.541	160
TS 3659	0.590	95
WC 231	0.590	80

Several observations are made from the dynamic and quasi-static data in Figure 7. The first is that the ball propellants are strain rate sensitive; that is, they are more difficult to compact dynamically than quasi-statically, with the largest differences occurring in the middle of the compaction range (~80% TMD). Another observation is that while quasi-static compaction of the NC propellants was minimally affected by particle size, dynamic compaction was considerably more difficult for the larger WC 140 particles. A third observation involves the effect of NG. Quasi-static compaction became significantly easier with increasing NG content (0% for Fluid A and WC 140, 21.6% for TS 3659, ~25% for WC 231). Dynamic compaction was also easier when increasing NG content from 0% to 21.6%. On the logarithmic scale of p in Figure 7, the relative change in p between WC 140 and TS 3659 at a given %TMD is greater for quasi-static versus dynamic compaction; however, the absolute change in p is approximately maintained between quasi-static and dynamic compaction of these materials.

Some early discussions of compressive reaction in ball propellants, while confined in Lexan tubes, were included in References 15 and 31. Following that, PDC experiments on TS 3659 and WC 140 in mostly aluminum and steel tubes were conducted in preparation for a JANNAF sponsored workshop[38] on modeling compressive reaction. All of the compaction and compressive reaction data for TS 3659 and WC 140 were described in detail in References 12 and 13, respectively, and summarized in Reference 14. That summary also contains the results of a 220-m/s impact on WC 231 (Shot PDC-73) in a Lexan tube that had a NaCl window for recording IR emissions from the compacting/reacting bed. The IR radiometry was complemented by high-speed photography and flash radiography within the same experiment.

Luminosity from weak reaction was observed from the rolled WC 231 powder at even the lowest compaction pressure, 14.8 MPa in Shot CGC-23, and more intense luminosity from vigorous reaction was observed at compaction pressures >50 MPa. By contrast, no luminosity was observed from the spherical TS 3659 powder, which has the same NG content as WC 231, over a range of compaction pressures from ~50 to ~100 MPa (Shots PDC-76, -77, -78). For an impact velocity of 291 m/s (Shot PDC-78), the backlighting of the piston noticeably decreased 83 μs after bed impact from what was assumed to be TS 3659 reaction products flowing between the inner wall and the piston. The tube ruptured, either from reaction pressure or from the high compaction pressure, as happened in the ~270-m/s impact on 60% TMD Teflon 7C (Shot PDC-2).[9] No attempt was made to use high-speed photography for observing reaction in impacted beds of WC 140 because it is less reactive than TS 3659. In Fluid A, which is a much smaller particle size NC powder than WC 140, luminosity was not detected by high-speed photography in Shot PDC-24, even though strain gauges recorded late reaction after the compaction front had reflected at the far end.

Prompt compressive reaction did not occur in any of the WC 140 experiments in even steel tube confinement.[13,14] Hence, observations concerning compaction and compressive reaction could be clearly distinguished. The first high confinement experiment (Shot PDC-71) was instrumented with only self-shorting probes, which recorded a SCW overtaking the compaction front 152 mm from the impacted end of the bed. The development of the SCW was observed in subsequent experiments (Shots M-30, -31), which were instrumented with self-shorting and ionization probes, pressure transducers, and the MI. For the 210-m/s piston impact in Shot M-30, the compaction front had a constant 563-m/s velocity for the 146-mm bed length and was never overtaken by the SCW (Figure 8a). The low range of pressure data from transducers at 38.4 mm (P_1) and 76.4 mm (P_2) are plotted in Figure 8b.

Several observations, which also apply to other experiments, can be made about the response of the transducers in Figure 8b. Note that the observed pressures are radial pressures on the inner wall, not the axial pressure driving the compaction front. The risetime of the front pressures (10.0 μs for P_1 and 9.5 μs for P_2) correspond to a maximum front thickness of 5.6 mm; however, the actual thickness may be less considering that the piezoelectric sensing area is 4.0 mm in diameter. The peak values of p_w, 65.9 MPa at P_1 and 61.1 MPa at P_2, declined slightly as the front propagated from P_1 to P_2; therefore, reaction pressure was not yet compensating for the loss of piston momentum and wall friction. Following each peak there was a rapid decline in p_w such that by the time

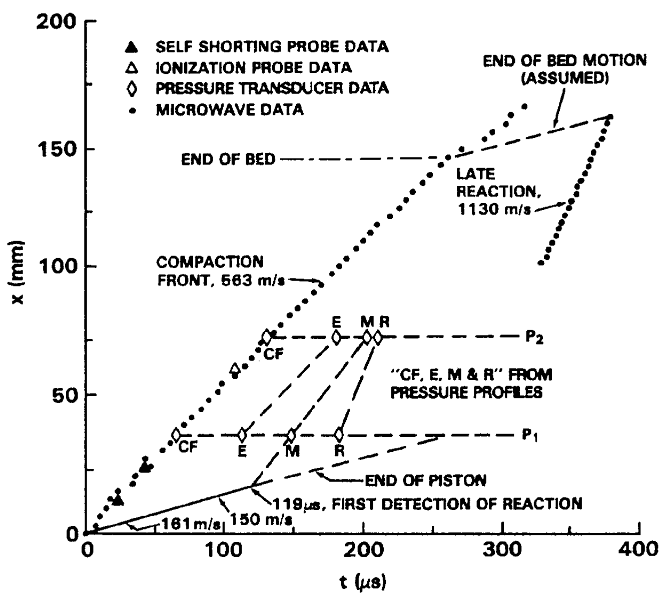

a. Summary of distance-time data

Figure 8. Data from a 210-m/s Impact of 60.5% TMD WC 140 Ball Propellant in a Steel Tube (Shot M-30)

that the CF reached P_2, the P_1 pressure was only about half of the peak CF pressure at P_2. While some decline in axial pressure occurs, as shown in Table IV for experiments with multiple front and particle velocity measurements, p_w may also decline because of the compacted bed sliding across the slightly recessed transducer, as discussed for Figure 4b. The end of the rapid decline in pressure behind the CF, denoted by the points 'E', forms a line parallel to the CF in Figure 8b. Similar pressure declines behind the CF were also observed in WC 140 Shot M-31 and TS 3659 Shot PDC-81, which had about the same impact velocity as in Shot M-30, For the lower (160 m/s) velocity impact in TS 3659 Shot PDC-80, there was very little pressure decline after passage of the CF (Figure 3 of Reference 12).

Increasing the piston impact velocity from 210 m/s in Shot M-30 to 300 m/s in Shot M-31 still resulted in reaction so delayed that the SCW did not overtake the compaction front before the end of the 146-mm-long bed. Compressive ignition of WC 140 is so marginal that the measured Δt increased rather than decreased for a piston impact velocity of 300 m/s versus 210 m/s. This was not the case for a spherical powder of nearly the same particle size that had NG added to the NC base, as discussed next for experiments on TS 3659.

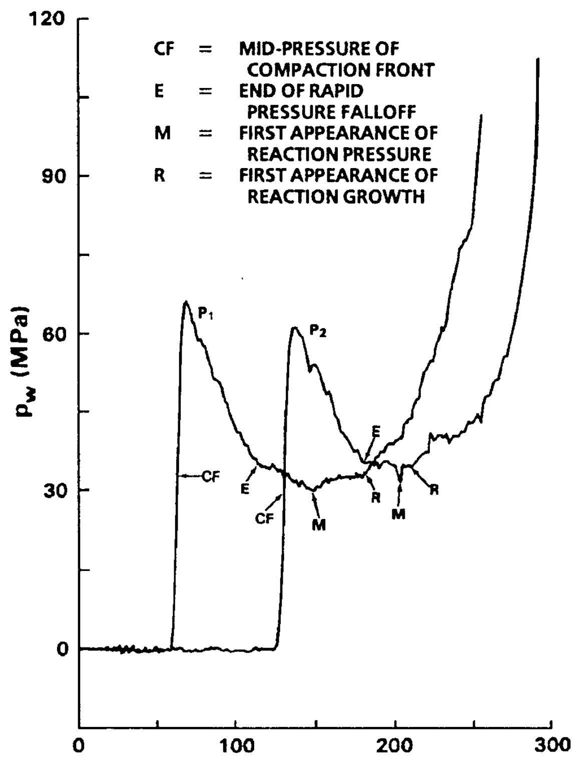

b. Inner wall pressures at 38.4 mm (P_1) and 76.4 mm (P_2)

Figure 8. Data from a 210-m/s Impact of 60.5% TMD WC 140 Ball Propellant in a Steel Tube (Shot M-30) (Continued)

The onset and growth of compressive reaction in ball propellants are illustrated by the results from two experiments with TS 3659 confined in steel tubes. These experiments were instrumented with piezoelectric transducers at 38.1 mm (P_1) and 76.2 mm (P_2), ionization and self-shorting probes, MI, and streak photography of the impacting piston. The lower impact velocity, 237 m/s in Shot PDC-81 resulted in a steady 534-m/s compaction front that promptly transited to a 1800-m/s reactive front just ~13 mm from the end of the 147-mm-long bed, as shown in Figure 9a. The pressure profiles in Figure 9b are initially the same as those for the inert compaction of melamine in Figure 4b; that is, the pressure promptly increased with the compaction front and then monotonically decreased. The pressure decline ended by 120 μs at P_1 and 178 μs at P_2, presumably as compressive waves from reaction near the piston reached those transducer locations. This is certainly the case at P_2 since the pressure immediately began to increase after 178 μs, as denoted in Figure 9b with an 'R', whereas the pressure at P_1 remained steady between 120 and 150 μs before beginning to increase. Assuming the end of the pressure decline at 120 μs for P_1 was the first appearance of reaction, the extrapolated line in Figure 9a between this point and 178 μs at P_2 provides a prediction of 84 μs for Δt. This is the value reported in Table V for Δt, rather than 140 μs obtained by extrapolating through the beginning of the P_1 pressure rise at 150 μs.

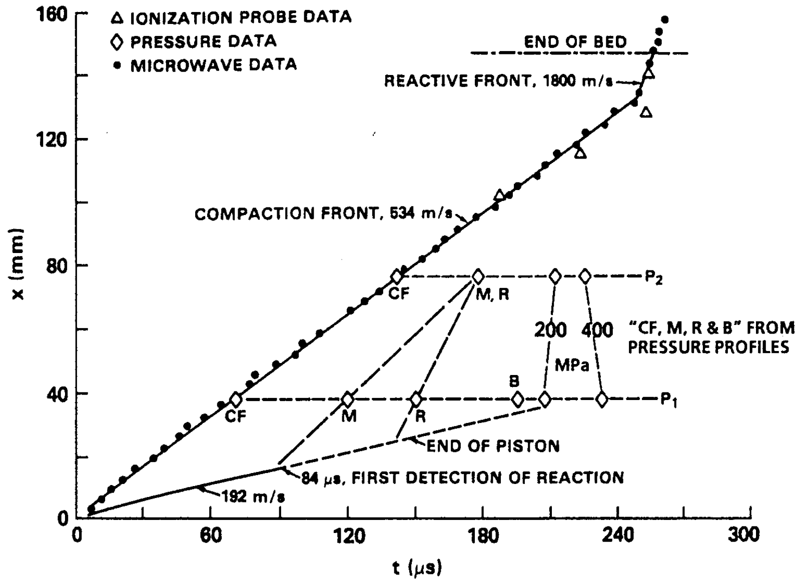

a. Summary of distance-time data

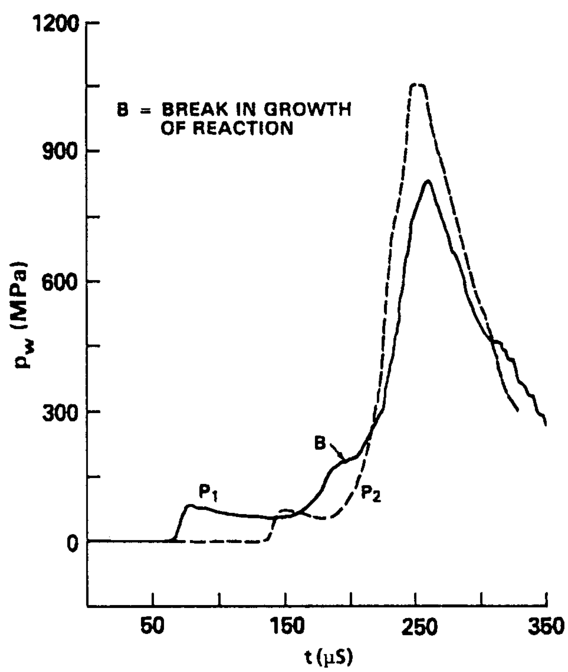

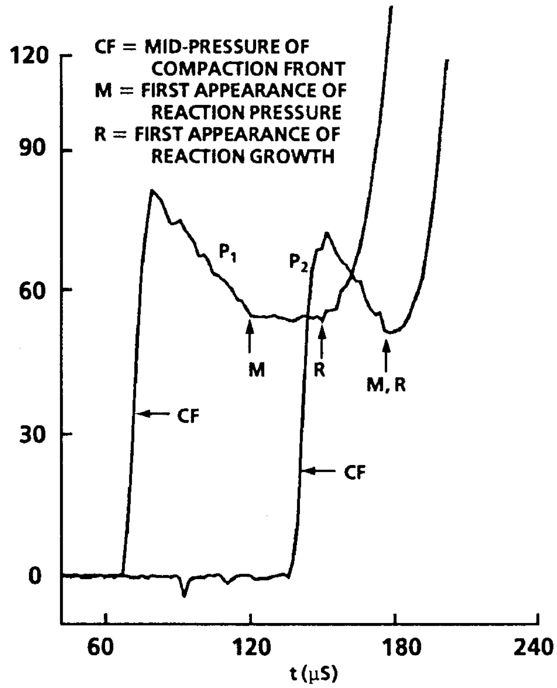

b. Low range inner wall pressures at 38.1 mm (P_1) and 76.2 mm (P_2)

c. High range inner wall pressures at 38.1 mm (P_1) and 76.2 mm (P_2)

Figure 9. Data from a 237-m/s Impact of 60.1% TMD TS 3659 Ball Propellant in a Steel Tube (Shot PDC-81)

Pressure buildup following the onset of reaction is plotted in Figure 9c with an increased pressure range. Except for a break in the P_1 trace, as denoted in Figure 9c with a 'B', the pressure at both locations steadily increased near to or in excess of the 0.86-GPa limit of the transducers. Although actual pressures may have been higher, these steel tubes begin plastically yielding at 0.22 GPa; thus, the observed pressures are limited by tube expansion as well as by transducer failure. The growth of reaction led to the formation of an SCW, which overtook the compaction front ~13 mm before the end of the bed. Only for the final four ionization probes (from 101.7 to 139.8 mm) was there enough ionization from reaction at the front to trigger them. This, along with the extrapolation of the isobars on Figure 9a to the front, indicate that the compaction front was increasing in strength. Note that compaction front velocity, which is a relatively insensitive measure of pressure, did not increase until the abrupt transition in velocity near the end of the bed.

A shorter Δt, followed by greater growth of reaction, resulted from a 300-m/s impact on TS 3659 in Shot PDC-82. The piston velocity prior to impact was similar to that for a Lexan tube experiment (Shot PDC-78) discussed previously, but the steel tube permitted a violent reaction to develop. As shown in Figure 10a, the 557-m/s compaction front near the impacted end of the bed had become an accelerating reactive front with a velocity of 2110 m/s at the far end of the bed. The pressure traces in Figure 10b have the same pressure scale and were obtained from the same locations as the traces in Figure 9c for the previously discussed experiment. In Shot PDC-82, rapid growth of reaction occurred as the front propagated from P_1 to P_2, and yet the front velocity was just beginning to accelerate (Figure 10a). The P_1 trace in Figure 10b is a typical compaction front profile, with ‘CF’ denoting the mid-pressure associated with the front, except that the pressure immediately behind the front continued to slowly increase rather than decline. This was the first indication of early reaction, and then within ~15 μs of the front passing P_1 the pressure began increasing more rapidly from growth of reaction, which is denoted in Figure 10 with an ‘R’. The pressure at P_1 then increased to ~400 MPa, where it remained relatively steady until after the front had passed P_2. With the arrival of the front at P_2, the transducer there recorded a very rapid rise in pressure to ~1 GPa, exceeding the limit of the transducer and indicating that the front had become a reactive shock wave. (The equally rapid decline in pressure at P_2 following the peak was due to transducer failure.) Pressures at P_2 probably remained high and drove compressive waves back to P_1, as recorded by the final rise in pressure at P_1 to ~750 MPa. As the front reached P_2 in Shot PDC-82, there was a significant increase in the amplitude of the microwave signal that reflected from the front due to ionization. This was attributed to an increase in the concentration of hot spots with high enough temperature to initiate reaction.[44,45] Another indication of the rapid pressure buildup when the front reached P_2 is that the piston had been arrested and was beginning to be pushed backwards.

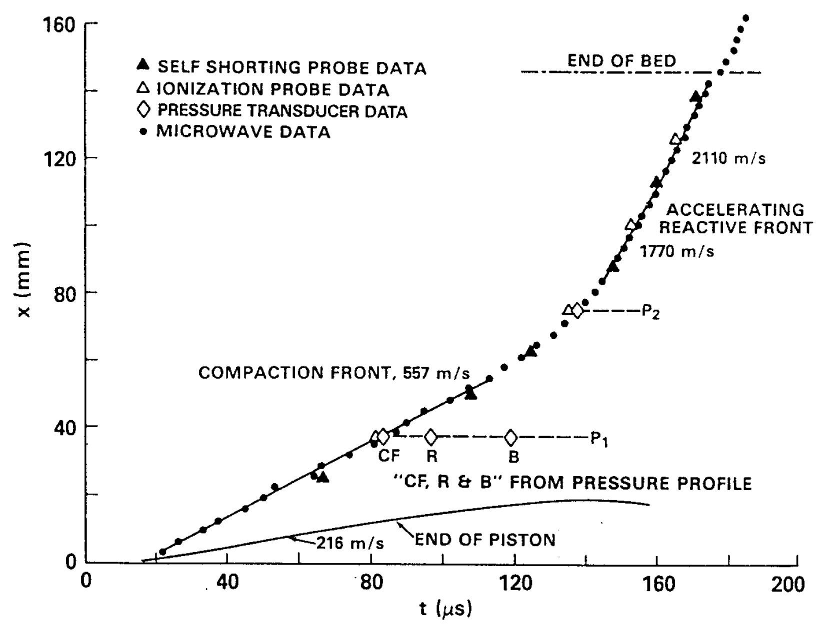

a. Summary of distance-time data

Figure 10. Data from a 300-m/s Impact of 60.1% TMD TS 3659 Ball Propellant in a Steel Tube (Shot PDC-82)

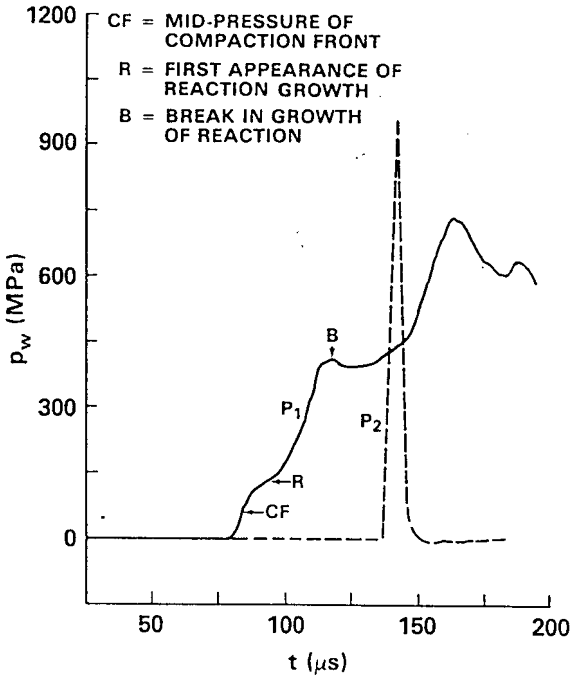

b. Inner wall pressures at 38.1 mm (P_1) and 76.2 mm (P_2)

Figure 10. Data from a 300-m/s Impact of 60.1% TMD TS 3659 Ball Propellant in a Steel Tube (Shot PDC-82) (Continued)

High-Energy Propellants

Experiments on three high-energy propellants, all impacted with Lexan pistons, are listed in Table VII. ABL 2523 casting powder was difficult to compact, like the ball propellants; it could be hand pressed to only ~65% TMD. HEP “X” and RS 075 were easily compacted by hand, allowing both to be investigated at initial packings of ~59% and ~75% TMD. All of the experiments listed in Table VII have been previously reported. The PDC shots on ABL 2523 and HEP “X,” and those on RS 075 up to and including Shot PDC-48, are summarized in Reference 15. Details of many of those experiments are discussed in Reference 32. The remaining RS 075 experiments listed in Table VII, Shots PDC-65 through PDC-68, were among the low amplitude shock initiation experiments reported in Reference 33.

Table VII. Summary of High-Energy Propellant Experiments

MATL.	SHOT	%TMD$_o$	L (mm)	TUBE	v_p (m/s)	u (m/s)	U (m/s)	%TMD	p (MPa)	Δt (μs)	COMMENTS
	INITIAL CONDITIONS					RESULTS					
ABL 2523 (HEP "Y")	PDC-52	64.4	133	Alum.	76	56 56 52	335 359 285	77.4 76.4 78.7	23.1 24.8 18.1	<262	Weak Reaction
	PDC-55	64.4	133	Alum.	137	118 154	448 476	87.4 95.2	64.6 89.5	<121	Moderate Reaction
	PDC-40	64.9	146	Lexan	192	131	460	90*	74	18	Moderate Reaction
	PDC-43	64.9	152	Steel	219	160	497	95*	98	<64	x_D = 140 mm
	PDC-47	64.9	178	Steel	284	194	545	100*	130	<20	x_D = 132 mm
HEP "X"	PDC-18	58.5	146		165	150	360	100*	59	20	x_D = 50 mm
	PDC-14	58.5	137	Lexan	200	180	430	100*	89	5	x_D = 55 mm
	PDC-15	74.5	296		~190	~180	710	100*	178	---	x_D = 39 mm
Short Shreds	PDC-34		133	Lexan	75	68 70 65	159 154 154	104.5 109.6 103.4	12.0 12.0 11.1	579	Weak Reaction
	PDC-36		133	Lexan	103	91 96 90	214 220 204	104.4 106.1 107.0	21.5 23.3 20.3	320	Weak Reaction
	PDC-35		133	Lexan	129	113	280	100*	35	36	Vigorous Reaction
	PDC-38		178	Steel	130	113	280	100*	35	<81	x_D = 127 mm
RS 075 (HEP "Z")	PDC-37	59.8	133	Lexan	~270	~210	520	100*	120	---	Vigorous Reaction
	PDC-44		152	Steel	~270	~210	520	100*	120	<15	x_D = 76 mm
	PDC-48		127	Steel+	294	207	515	100*	117	8.5	x_D = 73 mm
	PDC-68		98	Steel	354	242	602	100*	160	4	x_D = 61 mm
	PDC-66	75.0	146	Steel	161	95	380	100*	50	6	x_D = 76 mm
	PDC-65	75.0	134	Steel	248	128	512	100*	90	12	x_D = 74 mm
	PDC-67	75.0	110	Steel	353	260	1040	100*	373	1.4	x_D = 69 mm
Long Shreds	PDC-32	59.8	146	Lexan	270	210	520	100*	120	~9	Vigorous Reaction
	PDC-33	59.8	101	Lexan	270	200	500	100*	110	~9	Vigorous Reaction

* Assumed %TMD and measured u used in calculations for U and p

+ High strength steel versus mild steel

The onset of compressive reaction and the initial growth of reaction in all three high-energy propellants was rapid, compared to the explosives and ball propellants. Also, compressive reaction occurred in each experiment, even at the lowest piston velocity of ~75 m/s. The pressures associated with the reaction front from a 129 m/s impact of RS 075 in a steel tube (Shot PDC-38) are shown in Figure 11. The front pressure increased from 35 MPa at the driven end to 290 MPa at 38.1 mm to >530 MPa at 76.2 mm. Streak camera records are shown in Figures 12a and 12b, respectively, for PDC experiments on HEP "X" and RS 075 confined in Lexan tubes. In both experiments, a very luminous, reactive front had developed within 10 mm of the driven end. In HEP "X," the reaction front accelerated quickly and there was a distinct change in velocity at the onset of detonation, much like in HMX experiments. In RS 075, the reaction front velocity increased steadily as it propagated to the far end of the bed, where it was within 1 mm/μs of the detonation velocity in porous HEP "X" (Figure 12a). It can be assumed that the RS 075 would have detonated in a somewhat longer Lexan tube. In the one Lexan tube experiment with ABL 2523 (Shot PDC-40), reaction near the piston drove a steady 871-m/s luminous front down the length of the bed. This front velocity was higher than that from weak reaction in other experiments, and yet there was no acceleration of the front as occurs for vigorous reaction. In Table VII, a "moderate" level of reaction is associated with ABL 2523 Shot PDC-40. Moderate reaction is also associated with a higher velocity impact on ABL 2523 in intermediate confinement (Shot PDC-55), in which the aluminum tube violently ruptured after an ignition delay.

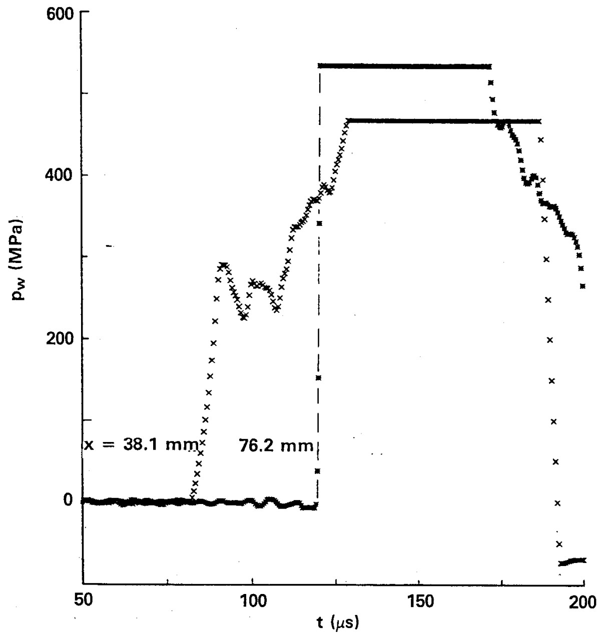

Figure 11. Inner Wall Pressures at Two Locations Following a 130-m/s Impact of 59.8% TMD RS 075 Propellant Shreds (Shot PDC-38)

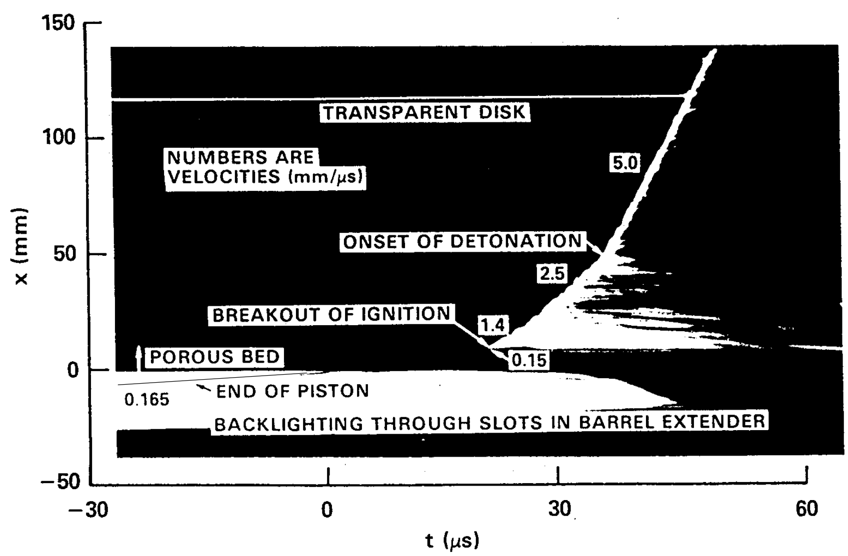

a. 165-m/s impact of 58.8% TMD Hep "X" (Shot PDC-18)

Figure 12. Streak Camera Records from Piston Impacts on Shredded High-Energy Propellants in Lexan Tubes

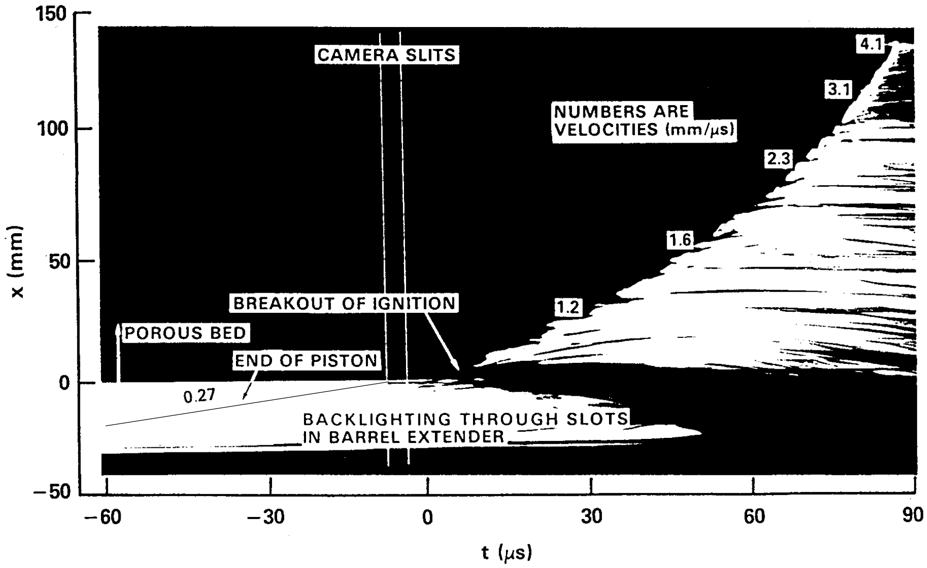

b. 270-m/s impact of 59.8% TMD RS 075 (Shot PDC-32)

Figure 12. Streak Camera Records from Piston Impacts on Shredded High-Energy Propellants in Lexan Tubes (Continued)

In steel tube confinement, the reaction front gradually accelerated in both ABL 2523 and RS 075, much like it did for Lexan tube experiments on RS 075. Figures 13a and 13b contain pin probe data for the reaction front in highly confined beds of ABL 2523 and RS 075, respectively. In these figures, distance and time are plotted relative to the onset of detonation ($x^* = x - x_D$ and $t^* = t - t_D$), where t_D is the time between bed impact and onset of detonation. For each material, the path of the developing shock front was insensitive to the piston impact velocity and even insensitive to differing bed packings for RS 075 (59.8 and 75.0% TMD). These materials transited to detonation in each steel tube experiment, over a range of piston velocities from 130 to 354 m/s. Except for a mild 130-m/s impact on RS 075 in Shot PDC-35, x_D was also relatively insensitive to v_p. For 59.8% TMD RS 075 impacted at ~280 m/s, the high strength steel tube in Shot PDC-48 did not result in any significant change in x_D when compared to the mild steel tube in Shot PDC-44.

Dynamic compaction data were obtained only for ABL 2523 and RS 075 from two low velocity impacts on each material because of the prompt onset of compressive reaction at higher velocities. Flash radiographs of tracers in those porous beds were analyzed for bed compaction (Table VII). In the lowest velocity impact on ABL 2523, Shot PDC-52 with v_p = 76 m/s, weak reaction appeared in the last (fourth) radiograph as a zone of reduced density near the compaction front. This zone was neglected in determining the average compaction parameters between the third and fourth radiographs, which are the third set of parameters listed for Shot PDC-52 in Table VII. Those parameters, which represent the first ~70% of the compacted bed, indicate that the piston was slowing slightly and that the front, if there would have been no reaction near it, would have slowed from ~350 to 285 m/s. Instead, the front had accelerated to 386 m/s. Unlike Shot PDC-52, in the next higher velocity impact on ABL 2523, Shot PDC-55 with v_p =137 m/s, the tabulated compaction data were affected by compressive reaction. Reaction near the piston in the third radiograph, which appeared as a zone of reduced density, had increased the compaction pressure over that imparted by the piston. The zone of increased compaction had not begun reacting yet and so was used in determining the second set of parameters that are tabulated for Shot PDC-55 in Table VII.

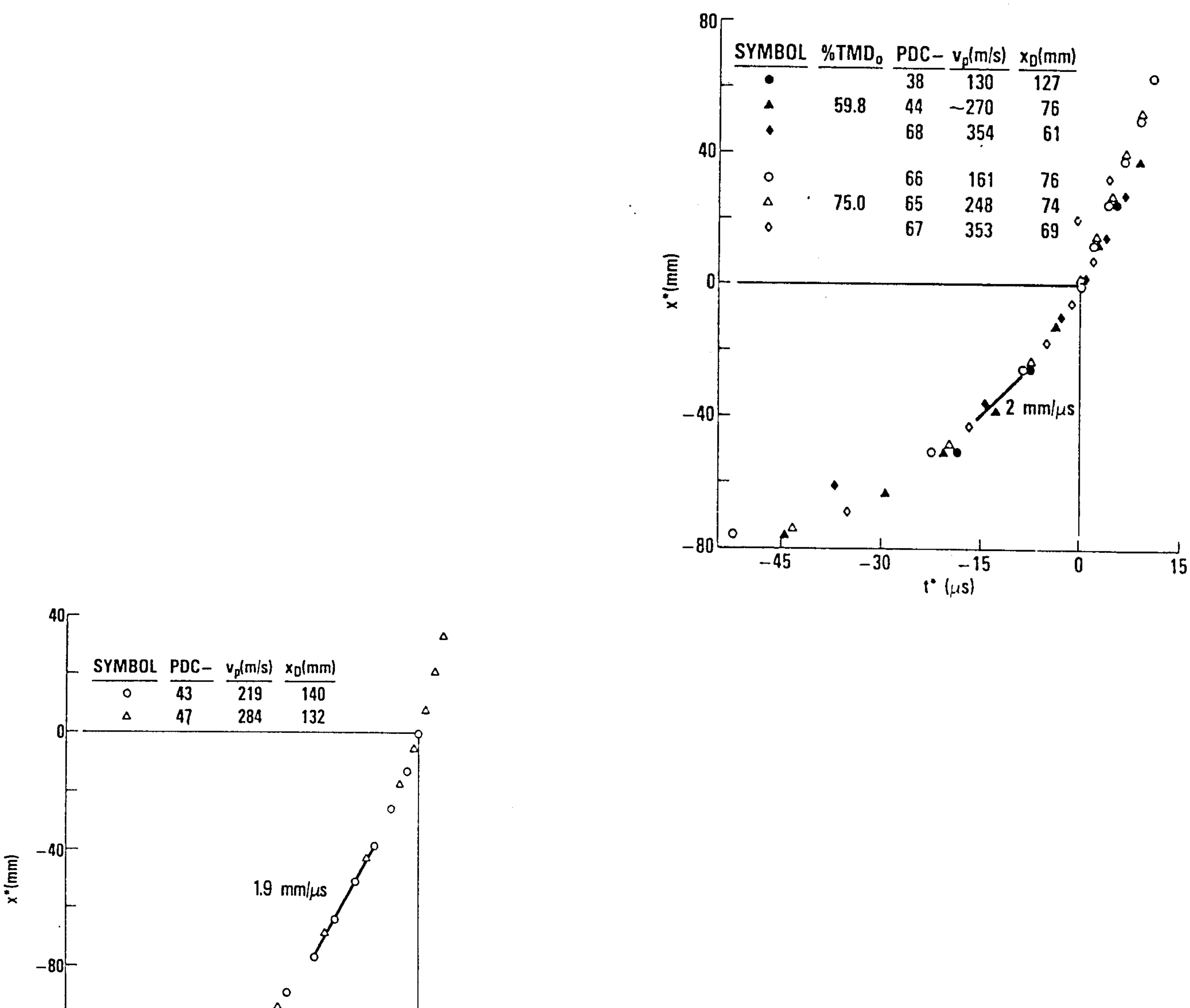

a. 64.9% TMD ABL 2523 **b. Two bed densities of shredded RS 075**

Figure 13. Reaction Front Position Versus Time (Both Relative to the Onset of Detonation) for Piston Impacts on Two High-Energy Propellants

The quasi-static data[21] for ABL 2523 are plotted in Figure 14 along with the dynamic measurements in aluminum tubes from Shots PDC-52, -55. As previously shown for the ball propellants in Figure 7, ABL 2523 is more difficult to compact dynamically than quasi-statically. An attempt was made to fit the quasi-static data with the lattice compaction model, as done for the ball propellants, even though the ABL 2523 particles are cylindrical instead of spherical. As shown in Figure 14, the model fit describes the data up to about 85% TMD, but underpredicts the data for higher extents of compaction. Also shown is a model fit through the dynamic data, which requires an increase in p_y from 90 MPa for quasi-static compaction to 150 MPa.

Dynamic compaction measurements from 75- and 103-m/s impacts on RS 075 (Shots PDC-34, -36) are discussed in Reference 16, along with the quasi-static compaction data. In agreement with the quasi-static data, the beds in Shots PDC-34, -36 were fully compacted even though the calculated jump pressures were low (12.6 and 20.3 MPa, respectively) relative to DDT events. For a somewhat higher jump pressure of 35 MPa (Shot PDC-35), a compaction measurement was not possible because of the rapid onset of compressive reaction. HEP “X” beds were qualitatively similar to RS 075 as far as ease of compaction, but no quasi-static or dynamic measurements were made. Due to the ease of compaction of both HEP “X” and RS 075, compaction to TMD was assumed when calculating front pressures for Table VII, except for RS 075 Shots PDC-34, -36 where u and U were measured without any significant influence of reaction.

Dynamic compaction to TMD in HEP “X” and RS 075 with $v_p > 100$ m/s existed only momentarily, if at all, when the piston impacted because of the rapid onset of compressive reaction. One of the high velocity impacts on RS 075 (Shot PDC-33) was radiographed; the bed was purposely limited to a length of 101 mm to avoid damage to the flash x-ray heads and film cassette. The radiographs showed no indication of even a thin zone of fully compacted material at the front, and the relatively small compaction at the front decreased with time. When the reactive front was at 22 mm, the bed was compacted to 66.7% TMD; 41.8 μs later when the reactive front was at 90 mm, the bed was compacted to only 62.3% TMD, which is just above the initial 59.8% TMD packing. It appears that as soon as the bed began to collapse the gas products from compressive reaction filled the pores and thereby inhibited further compaction.

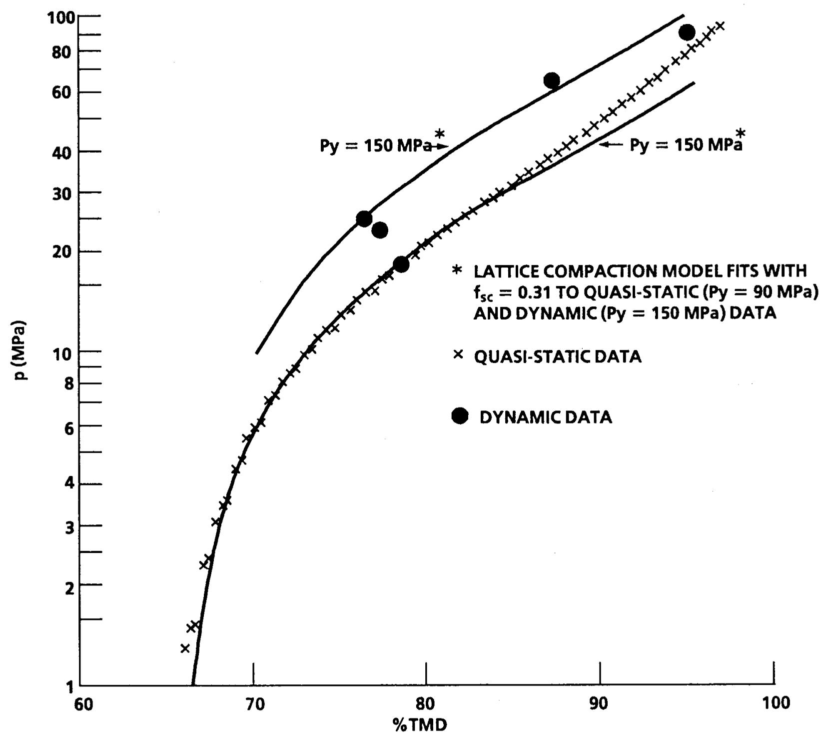

Figure 14. Compaction Data for ABL 2523

DISCUSSION

Dynamic Compaction

Dynamic compaction measurements, along with fitted quasi-static data, were shown for melamine, HMX, three of the ball propellants and ABL 2523 in Figures 3, 5, 7, and 14 respectively. Similar comparisons of dynamic and quasi-static data are shown for Teflon 7C in Figure 2 of Reference 10 and for RS 075 in Figure 14 of Reference 16. Such comparisons were originally made to determine if dynamic compaction could be modeled with a quasi-static constitutive relation, which is easier to obtain, or a modified quasi-static relation that accounted for strain rate effects. In early studies, it was shown that Teflon 7C was significantly more difficult to compact dynamically than quasi-statically.[7,10,11] This was attributed to a strain rate sensitivity effect, which was modeled by simply partitioning the compacted bed into elastic and plastic fractions.[24] No micromechanical model was developed which described the time dependent deformation of the bed particles. This model would be affected by the different compaction mechanisms—fracture for HMX crystals versus plastic deformation in ball propellants.

Elban and coworkers have determined the strain rate sensitivity for Teflon 7C,[24] HMX,[25] ball propellants,[26] ABL 2523,[26] and RS 075[16] from the stress relaxation that occurs following quasi-static compaction. For HMX crystals, which tend to fracture when compacted, the strain rate sensitivity was determined to be small; but as shown in Figure 5, the HMX beds were easier to compact dynamically, especially to greater than 90% TMD. Melamine also had a small strain rate sensitivity and appeared to be easier to compact dynamically above 90% TMD. Ball propellants were predicted[26] to have strain rate sensitivities much larger than those measured; and as shown in Figure 7, any effect from strain rate sensitivity was greatly diminished at the higher %TMDs. Thus it appears that melamine, HMX, ball propellants, and ABL 2523 respond to a mechanism at high %TMDs and high strain rates that counteracts the predicted strain rate sensitivity. Coyne and coworkers have recently suggested that thermal softening could be such a mechanism.[26] Kooker suggested[55] that the ease of dynamic compaction for melamine at high %TMDs, which are the most recent experiments, may be from softening of the melamine with age.

For the ball propellant compaction data shown in Figure VII, it appears that smaller particle size reduced strain rate sensitivity and that additional NG increased strain rate sensitivity. Stress relaxation measurements were not made for Fluid A (34 μm particle size), and so no model prediction of its strain rate sensitivity, relative to the larger WC 140 particles (411 μm), is available. Small particle size should reduce the scale of deformation at each particle-particle contact relative to larger particles in a bed compacted to the same %TMD. Speculating that greater deformation increases strain rate effects in a material, beds of small particles should be less strain rate sensitive. The beds of small (~50 μm) melamine particles were also relatively strain rate insensitive. While beds of small (~30 μm) Teflon 7C particles exhibited significant strain rate sensitivity, these beds were unlike the others in that they consisted of agglomerates of fibrous particles instead of individual balls or cylinders. In contrast to the measured effect of NG on dynamic compaction, the model for strain rate sensitivity predicted nearly the same stress to achieve ~83% TMD in beds of WC 140 and TS 3659, which have different NG contents for about the same particle size. It is speculated that softening the particles with NG may result in more uniform deformation without as much cracking and localized shear.

Dynamic compaction would also be influenced by any gases from compressive reaction that are generated as the pores collapse. The gases would stiffen the bed and have the same effect on compaction as strain rate sensitivity. Kooker calculated[39,56] that very small extents of reaction (often <1%) would account for observed differences between dynamic and quasi-static data, such as shown for the ball propellants TS 3659 and WC 140 in Figure 7. The greatest differences between dynamic and quasi-static data in Figure 7 occurred in the middle of the compaction range (~80% TMD). This is where significant plastic deformation occurs at particle to particle contacts without the neighboring contact surfaces impinging on each other. Both compressive reaction and strain rate effects would occur as a result of the deformation. If there was sufficient gas generation from reaction to make compaction more difficult, it is assumed that differences between quasi-static and dynamic data should diverge more at higher

%TMDs from a combination of increased reaction and less available pore volume for the gases. This was not the case, but Kooker suggested[55] that the immediate gasification from compressive reaction could be less at the higher %TMDs. Kooker's suggestion is based on the assumption that the increased strain rates accompanying the higher %TMDs in dynamic experiments would lead to a viscous layer at the particle contacts, which desensitizes the onset of reaction.

Another approach to presenting compaction data is to plot U versus u, as shown for Class D HMX and WC 140 in Figure 15. All of the Class D HMX data in Table III prior to the 267-m/s impact in Shot PDC-27 are included; compressive reaction occurred so quickly in the three experiments with the highest velocity impacts (225 to 267 m/s) that the U,u measurements may have had significant errors. The solid line in Figure 15a results from treating the quasi-static data as a Hugoniot and rearranging Equations 1 and 2 to calculate U and u. (A similar approach was used by Kooker; e.g., Figure 8a of Reference 56.) The quasi-static data used in the calculations were adjusted from that shown in Figure 5 by Kooker (Figure A-56 of Reference 56) to account for the higher initial packing density (73.0% TMD) in the dynamic experiments. The calculated front and particle velocities shown in Figure 15a are very nearly linear, U(m/s) = 112.4 + 3.366 u, much like the Hugoniots reported for many voidless materials. These calculated velocities from the quasi-static data agree with the dynamic measurements for the lower particle velocities, indicative of the small strain rate sensitivity predicted for Class D HMX. For the higher particle velocities, the somewhat lower dynamic front velocities indicate a softening of the HMX, as previously discussed for melamine.

All of the WC 140 dynamic U,u data in Table V are plotted in Figure 15b. Hugoniot calculations were made on quasi-static data that had been adjusted with the lattice compaction model to the initial packing density (60.5% TMD) of the dynamic experiments.[13] The solid line representing the Hugoniot calculations is not linear, but could be approximated as being linear with little error. However, there would be significant curvature in a line through the dynamic data. The differences between the dynamic measurements and the calculations on quasi-static measurements, especially in the middle of the compaction range, are even more apparent than in the p versus %TMD plot in Figure 7. The U versus u plot for WC 140 in Figure 15b even shows small differences at the lowest particle velocities, indicating some strain rate effect for minimal extents of compaction. However, Kooker's analysis of the same data did not show any differences at the lowest particle velocities (Figure A-9 of Reference 56) and thus no strain rate effect for initial compaction. The U,u predictions in Figure 15b and by Kooker do not agree because the calculations are very sensitive to the fit through the quasi-static data. As shown in Figure 16, there is little difference between Kooker's approximation (Figure A-8 of Reference 56) to Elban's quasi-static data and the lattice compaction model fit, with the initial packing density in both fits adjusted to 60.5% TMD. (Figure 16, as provided by Kooker,[57] is plotted in terms of mixture pressure and density, which includes any gases in the pores.)

The pressure transducers in recent experiments provided some new information about compaction, as well as verified[11] some earlier observations. They showed that the compaction front steadily propagated with little decline in peak pressure. This was previously thought to be the case based on near-constant front velocity, but U is an insensitive measure of p. The transducers also showed a decline in pressure behind the compaction front in several ball propellant experiments when reaction was not prompt.[12-14] Since a similar pressure decline behind the compaction front occurred in inert materials, both Teflon 7C[9] and melamine (Figure 4b), it appears that the effect is unrelated to reaction. The P_1 trace in Figure 4b suggests that some of the pressure fall behind the front may be because the slightly recessed transducer does not accurately record p_w once the bed begins sliding past its location. Two modelers[55,58] have attributed that fall off in pressure behind the compaction front in these experiments to rarefaction waves from the gradual slowing of the piston.

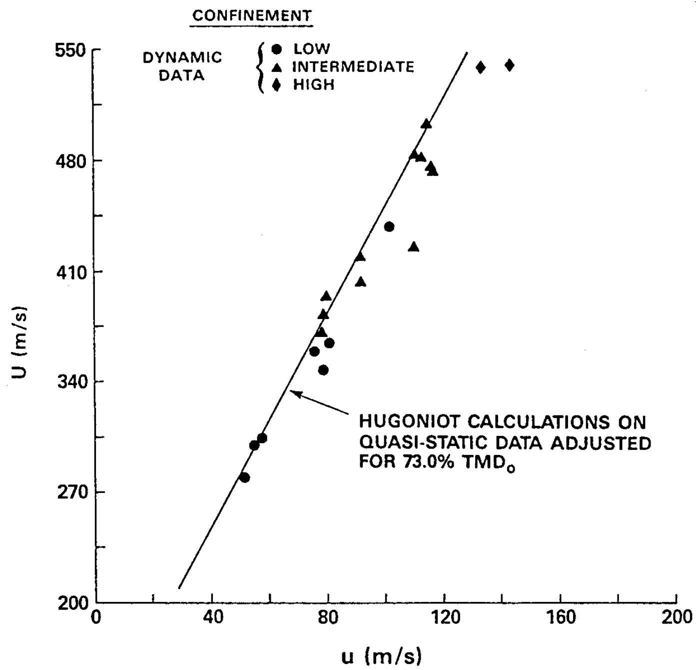

a. Class D HMX

b. WC 140 propellant, along with velocities predicted from quasi-static data

Figure 15. Front Versus Particle Velocities for Dynamic Compaction of Class D HMX and WC 140 Propellant

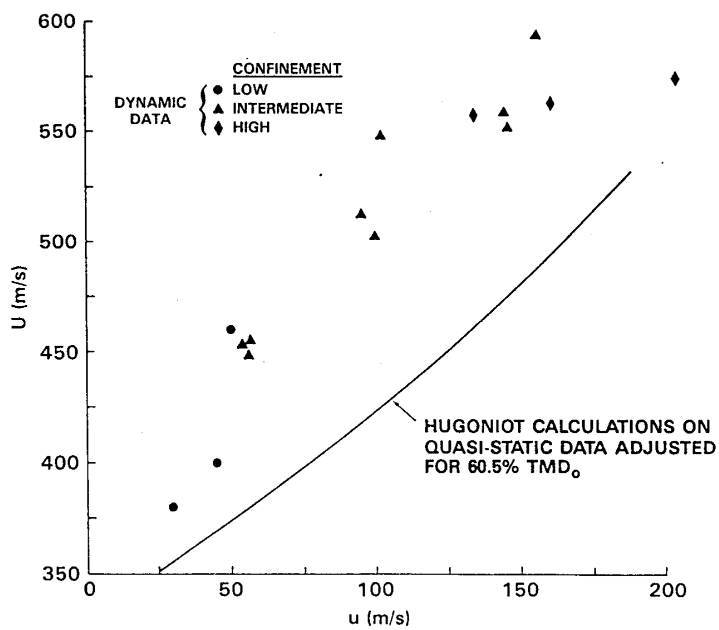

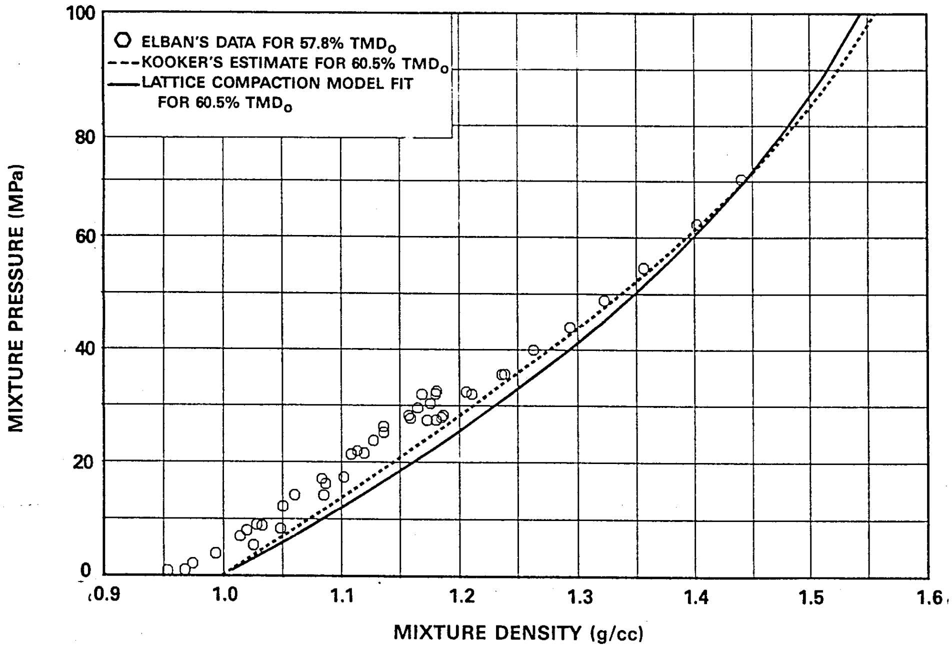

O ELBAN'S DATA FOR 57.8% TMD$_0$
---KOOKER'S ESTIMATE FOR 60.5% TMD$_0$
—LATTICE COMPACTION MODEL FIT FOR 60.5% TMD$_0$
MIXTURE PRESSURE (MPa)
0
20
40
60
80
100
0.9
1.0
1.1
1.2
1.3
1.4
1.5
1.6
MIXTURE DENSITY (g/cc)

Figure 16. Quasi-Static Compaction of WC 140 Propellant: Elban's Experimental Data for 57.8% TMD_o and Estimates Assuming 60.5% TMD_o as in Dynamic Experiments

The pressure transducers, however, did not improve the resolution of the compaction front thickness. Early flash radiographic measurements of metallic tracers in beds only resolved the thickness of the compaction front as no more than the 6-mm separation between the tracers; however, the fronts appeared to be much thinner (~1 mm) on the radiographs. The transducer data provided a maximum thickness for the compaction front of 5 to 7 mm based on the front transit time multiplied by U. The actual thickness may be less considering that the piezoelectric sensing area is 4.0 mm in diameter and oriented orthogonal to the wave passage; consequently, even a sharp front will appear as having a thickness of 4 mm.

Compressive Reaction

Compaction pressures associated with no detectable reaction, weak reaction, vigorous reaction, and detonation are summarized in Table VIII. Effects related to confinement and driver (cold gas versus Lexan or aluminum piston) are not specified but discussed subsequently. Weak reaction, as used here, is not accompanied by significant pressure buildup or acceleration of the front, whereas there is both pressure buildup and front acceleration with vigorous reaction. Since all of the energetic materials listed in Table I can detonate, vigorous reaction in any of these materials would eventually transit to detonation if there was sufficient confinement. Reaction commences with the generation of hot spots by the rapid deformation of the porous bed at the compaction front. Weak reaction is probably only partial reaction at some of the hottest and/or largest spots that does not spread to the cooler surrounding material; therefore, ignition (sustained reaction) has not occurred. Even though the extent of reaction and the number of participating hot spots is increased for vigorous reaction, there still may not be ignition of surrounding material near the driven end of the bed, where any reaction has had the longest time to develop. Compressive waves from the hot spot burn would coalesce with the compaction front, creating a SCW with more vigorous hot spot reaction that ignites surrounding material. At this point, the SCW would become a shock, and if confinement is not limiting further growth of reaction, a transition to detonation would occur.

Table VIII. Pressures Associated with the Levels of Compressive Reaction

(Summary of Tables III through V and VII)

Material	p (MPa) For Each Level of Reaction None	Weak	Vigorous	Detonation
Explosives				
HMX, Class D	23	38	-	66
HMX, #20 sieve cut	45	-	-	-
HMX, Class E	23	-	-	49
Tetryl, coarse	-	57	-	155
PBXW-108(E)	19,48	76	-	-
PBXW-109(E)	21	45-96	119?	-
Ball propellants				
Fluid A	20,49	42	-	-
WC 140	50	75	-	-
TS 3660	27	-	-	-
TS 3659	-	62	119	-
WC 231	-	15,26	60	168
High-energy propellants				
HEP "X"	-	-	-	59
ABL 2523	-	26,74	-	98
RS 075	-	13	35	35

There were usually too few experiments for each material to establish thresholds for weak reaction, vigorous reaction, and detonation. However, if the lowest pressure at which reaction was observed is associated with the threshold for weak reaction, it ranges from 12.6 to 76 MPa. Even though reaction was not observed for the #20 sieve cut of Class D HMX and TS 3660 ball propellant, the highest compaction pressures (45 and 17 MPa, respectively) were relatively low and reaction would presumably occur within the above range. Weak reaction occurred in two of the high-energy propellants, ABL 2523 and RS 075, at pressures less than in Class D HMX (37.5 MPa, Shot PDC-25). Since the lowest compaction pressure in HEP “X” (Shot PDC-18, p = 59 MPa) resulted in detonation, the threshold for weak reaction may be comparable to the other two high-energy propellants. Weak reaction was also observed in WC 231 at a relatively low pressure of 15 MPa.

There is a time delay, Δt, between bed impact and the detection of reaction that is listed in Tables III through V and VII for each experiment. The measurement of Δt was based on first reaction light on a camera film in low confinement experiments and changes in bed density in intermediate confinement experiments. In high confinement experiments, Δt was based either on ionization/self-shorting probe responses, pressure transducer records, or changes in piston velocity. The various techniques used in the intermediate and high confinement experiments resulted in only approximate measures of Δt relative to the direct observation of light in the low confinement experiments. It is of interest to correlate Δt with a compaction parameter in order to evaluate the time frame for participation of compressive reaction in DDT. One such correlation which is somewhat material independent is made with τ_i in Figure 17. The plot does not contain high confinement data because of the uncertainty in Δt; low confinement data for the PBXs and intermediate confinement data are plotted with left going arrows to indicate that Δt is less than that shown. Two lines corresponding to constant $\tau_i^2\Delta t$ are drawn on the plot; one line is characteristic of the explosives and WC 231, while the other line is characteristic of the high-energy propellants. At an equivalent τ_i, Δt for the high-energy propellants was approximately seven times less than for the explosives and WC 231. For intermediate and high confinement of TS 3659, estimates of Δt based on transducer measurements are consistent with WC 231, whereas Δt for WC 140 in high confinement was approximately twice that for WC 231 at the same τ_i. In WC 140, compressive reaction was so marginal that increasing v_p from 210 to 300 m/s somewhat increased Δt instead of decreasing it.

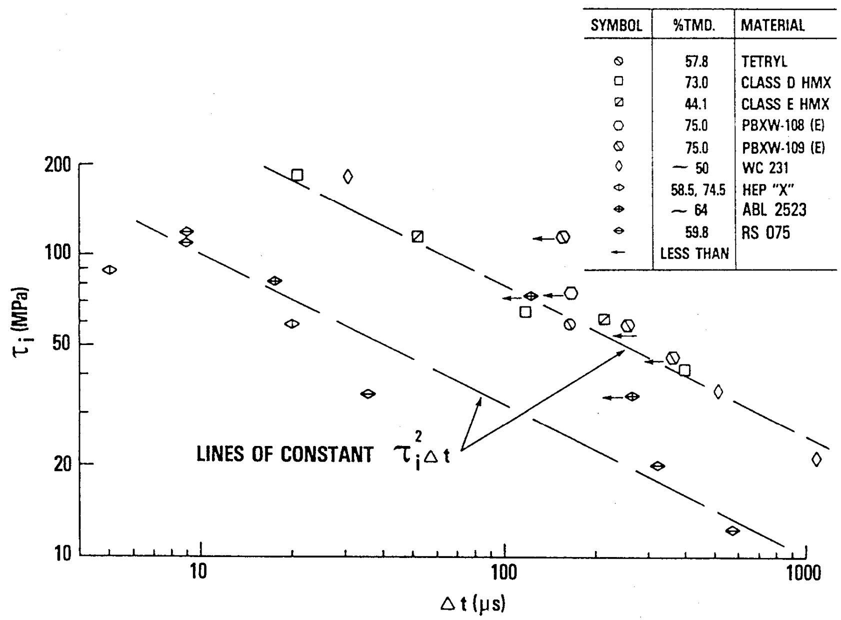

Figure 17. Average Solid Stress Versus Time for Detection of Compressive Reaction in Dynamically Loaded Beds

In low confinement experiments with continuous camera coverage, reaction was usually detected first at the driven end of the bed, whether the bed was compacted by an impacting piston or by pressurized gas.[15,31] Not only is the driven end the first part of the bed to be compacted, but the amplitude and rate of pressure rise is greatest there prior to growth of reaction further downstream. High-speed photography of beds confined in Lexan tubes was not always a definitive method of detecting first reaction. For beds of fine particles or beds that were highly compacted, reaction was not necessarily detected at the driven end. One explanation is that the pores were too small for the hot luminous gases to expose the camera film. Another possibility is that the initial reaction produced intermediates which were not hot enough to expose the camera film. This may have occurred in Lexan tube experiments on TS 3659, such as Shot PDC-78 where it is assumed that nonluminous reaction products began blocking the backlighting 83 μs after bed impact.[12]

The threshold for weak reaction was not expected to be a function of the experimental arrangement since each could confine the compaction pressures necessary to initiate reaction. There were, however, HMX experiments with all three arrangements near the threshold of reaction with various levels of reaction. For Class D HMX, weak reaction occurred in Lexan tubes at lower compaction pressures than in several experiments with supported thin-wall aluminum tubes. For both Class D and Class E HMX, detonation occurred in a steel tube at a lower compaction pressure than weak reaction in an aluminum tube. It was suggested in Reference 15 that a carbon gauge package on the end of the bed in some of the early intermediate confinement experiments may have reduced the sensitivity to reaction. Those gauge packages were removed in subsequent Class D HMX experiments with intermediate confinement. In a series of three Class D HMX experiments (Shots M-20, -21, -22), microwave interferometry and flash radiography both showed that reaction occurred near the driven end but extinguished. This may have been the same weakly luminous reaction which did not extinguish in Lexan tube experiments. Thus, even without a carbon gauge package, the aluminum tube arrangement inhibited compressive reaction in HMX relative to confinement by Lexan and steel tubes. Both the onset and growth of compressive reaction would be affected most by boundary conditions when near the reaction threshold. When near that threshold, reaction might occur at the inner wall of the tube because the initial pores are larger, which permits more deformation during compaction. The greater thermal conductivity of an aluminum wall would remove more heat and thereby inhibit reaction.

The threshold for vigorous reaction occurred at a somewhat higher range of pressures, 35 to 119 MPa (Table VIII), relative to the threshold for weak reaction. This range is exclusive of the two PBXs with inert binders, which probably have a higher threshold. Just as for the onset of reaction, the threshold for vigorous reaction was affected by the experimental arrangement. In Class E HMX, only weak reaction was observed in Lexan tube Shot PDC-46, whereas detonation occurred in steel tube Shot PDC-39 from a slightly lower compaction pressure. Since the compaction pressures were only ~50 MPa in these experiments, it is unlikely that confinement was responsible for all of the difference. In TS 3659, vigorous reaction was attained in both aluminum and steel tubes over the same velocity range as Lexan tube experiments, in which only weak reaction was assumed to occur for a 291-m/s impact.

The ball propellants permitted variations in composition (%NG) and particle condition (spheres versus disks rolled from spheres). WC 231 and TS 3659 had essentially the same composition, but WC 231 was more easily ignited and had greater growth of reaction, presumably because of damage to the particles from rolling during manufacture. WC 140 and TS 3659 were spheres of approximately the same size, but TS 3659 contained 21.6% NG while WC 140 had none. In steel tube confinement, WC 140 was more difficult to ignite and had slower pressure buildup during growth of compressive reaction than TS 3659. The high confinement TS 3659 experiments exhibited growth of compressive reaction much as in the final stages of DDT. The transducer records from Shot PDC-82 in Figure 10b are quite similar[53] to those from transducers located 133 and 89 mm before the onset of detonation in DDT Shot A268 on TS 3659.

MI and IR radiometer data obtained from the ball propellant experiments have provided additional insight into compressive reaction. Even as growth of compressive reaction in TS 3659 Shot PDC-81 increased the pressure near the impacted end of the bed to ~1 GPa, the transmission of microwaves was not interrupted. In WC 231 Shot PDC-73, the IR radiometer recorded the peak temperature as the compaction front passed its recording position; the subsequent decline in temperature even continued when a weakly luminous front passed about 50 μs later. Both measurements indicate that no new hot spots are being created in the compacted region of the bed, even after significant pressure buildup from reaction. Once the SCW from that pressure buildup overtakes the compaction front and forms an accelerating reactive front, the amplitude of the reflected microwave signal from that front rapidly increases. The most obvious explanation is both an increased number and size of hot spots, which reflect the microwaves. This explanation is supported by camera film records from WC 231 Shot PDC-73 and experiments on HMX. The SCW is weakly luminous as it propagates through the compacted bed, but becomes brightly luminous and accelerates upon overtaking the compaction front.

As previously noted, the high-energy propellants had low thresholds for compressive reaction and a short delay before the onset of reaction. Also, the initial growth of compressive reaction in the high energy-propellants was rapid, based on pressure records for RS 075 in Figure 11 compared to those for TS 3659 in Figure 10b, and as shown on the streak records for HEP "X" and RS 075 in Figure 12. The pressures from that early reaction (290 MPa at 38.1 mm in RS 075 Shot PDC-38, Figure 11) were greater than the highest impact pressures. Except for an ~10 mm zone of compacted bed at the piston, the position of the front was controlled by growth of compressive reaction. This is probably why x* versus t* was independent of v_p in high confinement experiments on ABL 2523 and RS 075, as shown in Figure 13.

Transition to Detonation

Those materials that transited to detonation in low-confinement piston-driven compaction experiments—HMX, tetryl, WC 231, and HEP "X"—also detonated in low confinement DDT experiments[4,48,52,54] at this Center. The growth of compressive reaction in these materials was rapid enough to overcome expansion of the Lexan tubes. Detonation occurred in every low confinement PDC experiment on HMX, tetryl, and HEP "X" in which vigorous reaction was initiated. In both WC 231 and RS 075, there were Lexan tube experiments in which vigorous reaction occurred without a transition to detonation, possibly because the bed was too short.

All the ball propellants had been investigated in steel tube DDT experiments.[48] Fluid A, TS 3659, and WC 231 transited to detonation, whereas WC 140 and TS 3660 did not attain detonation in bed lengths of 368 and 330 mm, respectively. Of these propellants, only TS 3659 and WC 140 were impacted in steel tubes at high enough piston velocities to assess their potential to detonate. For several reasons, TS 3659 did not detonate in the PDC experiments, whereas it had in DDT experiments. The steel ignitor plate in the DDT apparatus offers more confinement than the Lexan piston, which in Shot PDC-82 was being pushed back out of the tube after the onset of vigorous reaction. This would send rarefactions toward the reactive front, thus weakening it. Also, in the DDT experiments on TS 3659, at least 100 mm of run length existed between the formation of a strong reactive front and the transition to detonation. As shown in Figure 10a, a similar run length was not available; therefore, a longer tube may have permitted detonation. In PDC experiments on WC 140, the growth of compressive reaction was slower and occurred later than in TS 3659. Therefore, WC 140 would be less likely to detonate in DDT experiments, which is in agreement with its failure to detonate in a 368-mm bed length in a steel DDT tube.

The high-energy propellants ABL 2523 and RS 075 both transited to detonation in steel tube PDC experiments. No DDT experiments are available for comparison for these two propellants, but both would probably detonate in steel tube confinement. In RS 075, vigorous reaction was observed over a wide range of compaction pressures (35 to 120 MPa) in Lexan tubes without transiting to detonation, but probably would have detonated in a somewhat longer bed. In steel tube confinement, RS 075 transited to detonation at the lowest compaction pressure (35 MPa) where vigorous reaction was observed. There was no significant difference in x_D when using a higher strength steel tube that had been hardened (Shot PDC-48) versus a mild steel tube (Shot PDC-44). While it appears that steel tube confinement was not limiting the growth of compressive reaction, it should be noted that the reaction pressures greatly exceed the yield strength of even the strongest steels and that tube wall inertia is the important factor.

Run distance versus pressure is plotted for the explosives and propellants in Figures 18a and 18b, respectively. In addition to PDC data, these figures also contain measurements from other investigators on the same or similar materials, both in a porous state and near TMD. Lindstrom's wedge test measurements on 75.1% TMD tetryl[34] span an order of magnitude variation in shock pressure that just overlaps the higher pressure PDC data. These data are shown in both figures with a dashed line extrapolated into the lower pressures of the PDC data.

In Figure 18a, PDC data for Lexan piston impacts on 44.1% TMD Class E HMX confined in Lexan and steel tubes and for aluminum piston impacts on both 73.0% TMD Class D HMX and 75.1% TMD coarse tetryl confined in steel tubes are along that dashed line. The tetryl PDC data even extends into the pressure range of Lindstrom's measurements. Reducing the confinement on the end of Class D HMX beds by a Lexan piston impact in a either steel or Lexan tube resulted in data mostly above the dashed line; that is, the run distance to detonation is longer for a given pressure. Since Lexan begins to yield at ~70 MPa quasi-statically, it appears that these pistons were not able to maintain confinement on the end of the bed, especially once reaction began. The growth of compressive reaction in HMX, both Class D and Class E, is high enough that confining the beds with Lexan tubes did not result in increased x_D relative to steel tube confinement. Gap test data,[48] attained with a large scale gap test (LSGT) donor, for porous beds of coarse HMX and tetryl confined in plastic tubes are above the dashed line, probably because of the short shock pulse relative to the extended shock duration in PDC experiments and wedge tests. The only other wedge test data for porous beds, two data points for 65.2% TMD Class A HMX[50], exhibit about the same (slightly reduced) run distances as for 75.1% TMD coarse tetryl.[34] For wedge tests with near-TMD charges of HMX and tetryl, x_D increases rapidly with decreasing p, such that very long run distances would be required to obtain detonation in near-TMD charges at the pressures of the PDC experiments. The porous and near-TMD wedge test data tend to converge as x_D approaches the dimension of single crystals.

For the porous propellants, much of the x_D versus p data in Figure 18b could be approximated by a line that is parallel to and somewhat higher than the dashed line for 75.1% TMD coarse tetryl. All of the PDC experiments had Lexan piston impacts, which may have resulted in increased run distances relative to impacts with aluminum pistons, as occurred in 73.0% TMD Class D HMX. The gun impact experiments by Green and co-workers on 72.0% TMD Propellant “C”,[59] another high-energy propellant, had a steel impactor but plastic tube confinement. While both sets of experiments have limitations in confinement, increased run distances with respect to the dashed line may be from reduced growth of compressive reaction (i.e., shock reactivity) of propellants relative to neat HMX and tetryl. The x_D versus p data shown for wedge tests on near-TMD (cast) VTG-5A,[60] another high-energy propellant, are higher over the same pressure range than run distances in near-TMD HMX and tetryl (Figure 18a). Reduced growth of compressive reaction may also explain the invariance in x_D with p for 75.0% TMD RS 075, as shown in Figure 18b with a dotted line. As discussed in the previous section, the high-energy propellants promptly react (Figure 17) and generate pressures that quickly exceeds even the highest impact pressure (Figure 11); thereafter, the buildup proceeds at the same rate (Figure 13). If this buildup process is the limiting step in the transition to detonation, then x_D can be nearly equivalent for a range of impact pressures. Also note in Figure 18b that the gap test datum (LSGT donor) for WC 231 has about the same x_D as a lower pressure PDC experiment with similar confinement. This is equivalent to a longer x_D in the gap test at the same p, as shown in Figure 18a for HMX and tetryl.

The critical condition for initiation of detonation in high confinement corresponds to the threshold of vigorous reaction. For the various materials without an inert binder, that threshold occurred for a narrow range of particle velocities (113 to 160 m/s) relative to the corresponding range of compaction pressures (35 to 119 MPa). Roth suggested[61] that a relatively narrow range of particle velocities defined the critical conditions for SDT in gap and wedge tests on various densities of RDX, PETN, HNS, and tetryl. Whereas the critical pressures varied by a factor of ten (0.25 to 2.5 GPa), the critical particle velocities varied only by a factor of two (260 to 560 m/s). These particle velocities and pressures are higher than in the PDC experiments because of the shorter run distances to detonation and the narrower pulse width of the initiating shock in SDT studies. It is shown in Figure 19 that all of the x_D measurements fall within a band of constant slope when plotting x_D versus u for both porous and near-TMD materials. While the logarithmic plotting of x_D versus u in Figure 19 compresses the data and appears to improve the correlation, x_D versus p was also represented on logarithmic plots in Figure 18.

The high confinement PDC experiments may be viewed as a technique for studying one-dimensional buildup of weak shocks to detonation in porous samples. The PDC driver system is much smaller than Green’s 152-mm gun projectile[59] or a wedge test donor[60], and yet provides similar run distances to detonation. Increased x_D, indicating two-dimensional effects, occurred 160 g LSGT donors having two orders of magnitude more energetic material than a PDC driver.

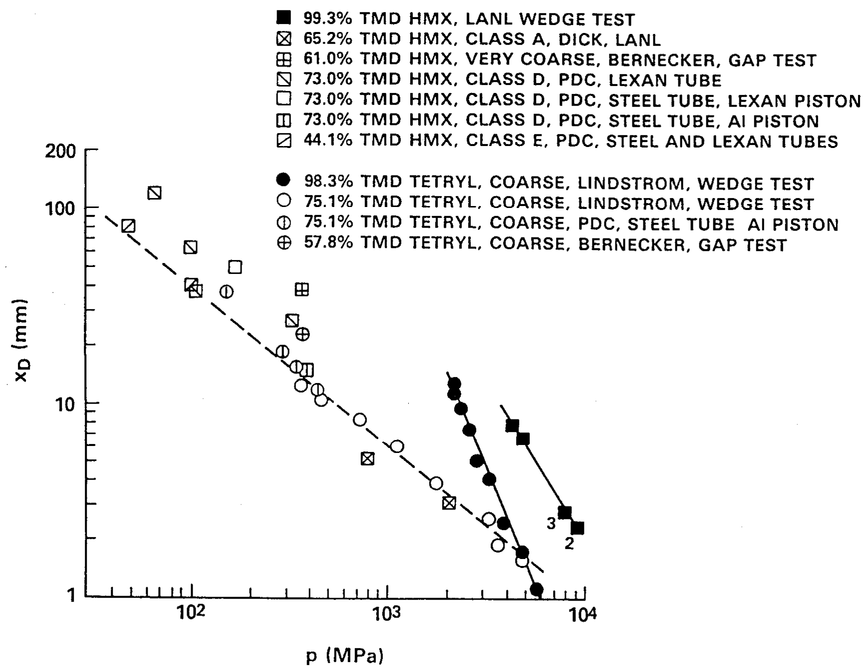

a. Explosives

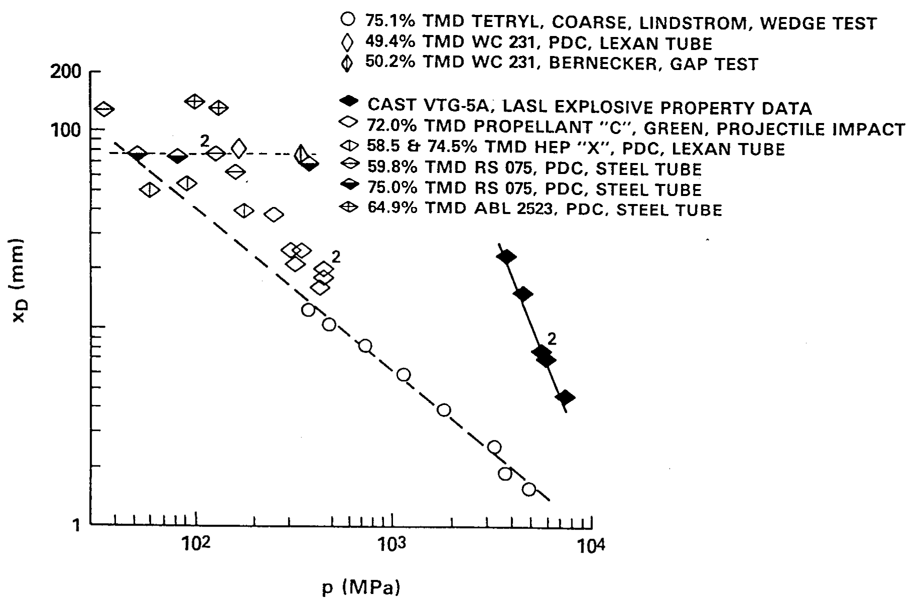

b. Propellants

Figure 18. Run Distance to Detonation Versus Pressure

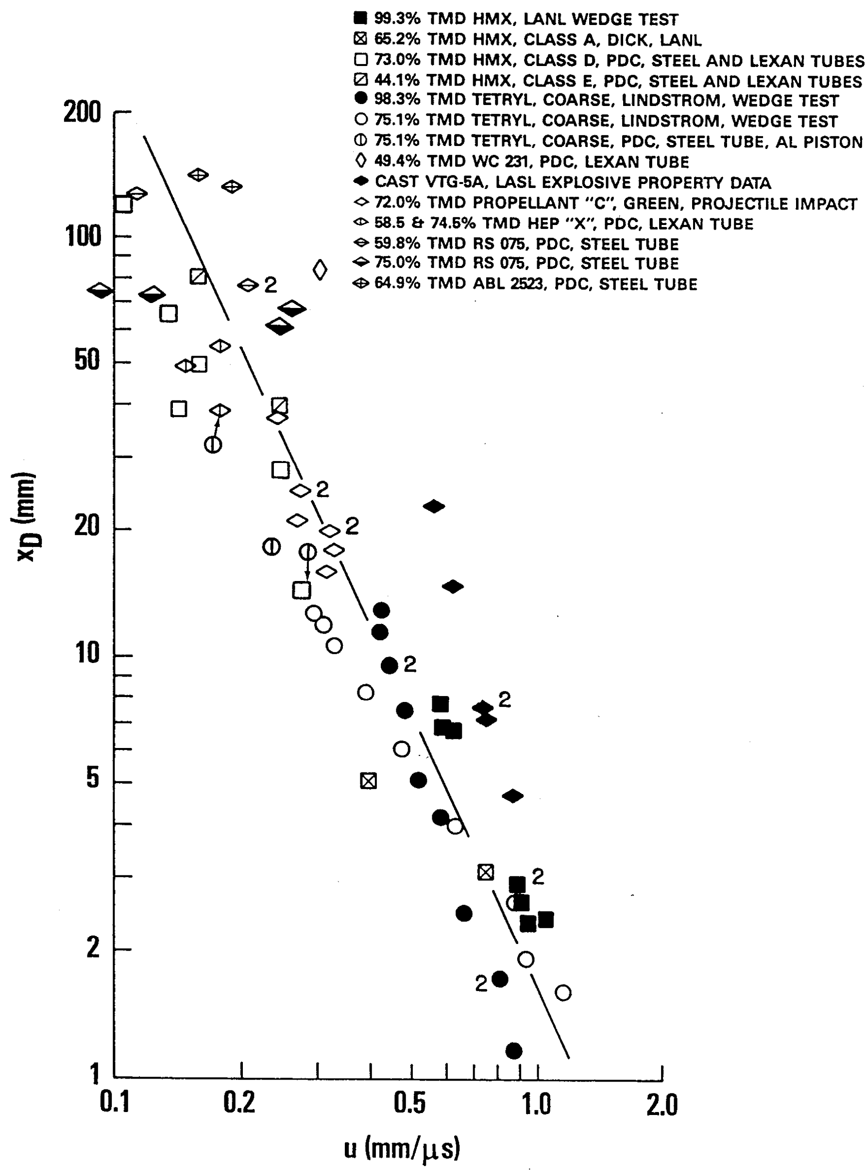

Figure 19. Run Distance to Detonation Versus Particle Velocity

SUMMARY AND CONCLUSIONS

Porous beds of both inert and energetic materials, ranging from 44.2% to 85.0% TMD, were dynamically loaded at pressures of interest to the various stages of DDT. These stages include the initial dynamic compaction of the bed without significant reaction, the onset of compressive reaction from rapid bed collapse, the growth of compressive reaction into a reactive shock, and finally the transition from a shock to detonation. Various techniques were developed for loading porous beds confined in cylindrical tubes, but most experiments utilized the PDC apparatus, which provided the range of input pressures corresponding to the above DDT stages by impacting one end of the bed with a long rod of either Lexan or aluminum. This loading technique applies a long duration pressure pulse, resulting in a quasi-steady wave that is ideal for correlating measurements with the pressure amplitude.

Dynamic compaction of porous inert materials was studied over a range of bed pressures from 15 to 300 MPa. The highest pressures imposed on energetic materials could not exceed the onset of vigorous compressive reaction, which ranged from 35 to 119 MPa depending on the material, to avoid significant influence from reaction. While compaction fronts steadily propagated with little decline in peak pressure, there was a significant decay in pressure behind the front that was attributed by modelers to a gradual slowing of the piston after bed impact. The flash radiographic images of fronts appeared to be thin, of the order of 1 mm. Direct measurements of front thickness by radiography of tracers in the porous beds and by pressure transducers had limited resolution, and it could only be determined that front thickness was not greater than 5 to 7 mm.

Quasi-static experiments by Elban et al.[16-26] complemented these dynamic compaction studies and provided a complete profile of load versus extent of compaction independent of material decomposition, although at much lower strain rates. Strain rate sensitivity of many of the materials was assessed, for the purpose of predicting compaction at the higher strain rates of the dynamic experiments, by evaluating stress relaxation following quasi-static loading. By this methodology, HMX was predicted to have little strain rate sensitivity, in agreement with the small difference between quasi-static and dynamic compaction data up to ~90% TMD. Ball propellants were predicted to be strain rate sensitive, but the predicted dynamic stresses were far more than the factor of two actually required to achieve the same extent of compaction quasi-statically up to ~90% TMD. For extensive compaction, >90% TMD, strain rate insensitive materials were easier to compact dynamically, and the increased difficulty of dynamic versus quasi-static compaction in strain rate sensitive materials was less. This occurred even when there was evidence of weak reaction in the energetic materials. Of the proposed explanations, thermal softening[26] at high strain rates is probably most viable. Any immediate gas generation from hot spot reaction during pore collapse would further stiffen a dynamically compacted bed, especially for extensive compaction when pore volume is small. This is the opposite effect of that observed, verifying other observations that weak reactions are delayed. Because strain rate sensitivity is somewhat balanced by a competing mechanism, such as the proposed thermal softening, quasi-static data provide a first approximation to dynamic compaction.

The threshold for compressive reaction in various energetic materials with porosities of 44% to 75% TMD ranged from 12.6 to 76 MPa, pressures which could be easily attained in an accident. It was found that the time for detection of reaction was inversely proportional to the square of the average solid stress. Vigorous reaction occurred at a somewhat higher pressures, ranging from 35 to 119 MPa, except possibly for two granulated PBXs with inert binders. With high confinement, vigorous reaction would build to detonation in less than 100 μs. With low confinement, higher compaction pressures were required to achieve detonation; even then, some materials failed to transit to detonation. Those materials which detonated in low confinement had also underwent DDT in low confinement experiments at the former White Oak Laboratory. The threshold for vigorous reaction occurred over a narrow range of particle velocities (113 to 160 m/s); a relatively narrow, but higher, range of critical particle velocities (260 to 560 m/s) was reported for SDT in gap and wedge tests. The run distances to detonation measured in this study are long, often >50 mm, relative to those in typical SDT studies. The long run distances reasonably agree with a linear extrapolation of data in the literature for SDT in porous materials to lower shock pressures.

The pressure required to collapse porous beds to >90% TMD does not exceed 100 to 200 MPa for the variety of energetic materials that were investigated. These pressures are exceeded considerably during buildup to detonation. Once the bed collapses, gas flow ahead of the burning zone is restricted, thereby slowing the pressure buildup by convective burning. However, collapse of the bed at high strain rates initiates compressive reaction, which can drive a sufficiently strong shock to achieve a transition to detonation. The experimental data support a model where a) hot spots are generated by the compaction process; b) reaction first occurs at the larger hot spots, often failing to propagate to surrounding material for the lower input pressures but still enhancing the front pressure; and c) at high input pressures, reaction occurs at both large and small hot spots and spreads to the surrounding material. The size, concentration, and temperature of the hot spots; the time before reaction occurs; and the rate of that reaction are dependent on the strength of the compaction front. If the reaction is vigorous and the confinement is adequate, the front will develop into a shock and then into a detonation.

REFERENCES

1. Bernecker, R. R. and Price, D., "Studies in the Transition from Deflagration to Detonation in Granular Explosives - II. Transitional Characteristics and Mechanisms Observed in 91/9 RDX/Wax," *Combustion and Flame*, Vol. 22, 1974, pp. 119-129.

2. Bernecker, R. R. and Price, D., "Studies in the Transition from Deflagration to Detonation in Granular Explosives - III. Proposed Mechanisms for Transition and Comparison with Other Proposals in the Literature," *Combustion and Flame*, Vol. 22, 1974, pp. 161-170.

3. Korotkov, A. I., Sulimov, A. A., Obmenin, A. V., Dubovitskii, V. F., and Kurkin, A. I., "Transition from Combustion to Detonation in Porous Explosives," *Combustion, Explosion, and Shock Waves*, Vol. 5, No. 3, 1969, pp. 315-325.

4. Bernecker, R. R., Sandusky, H. W., and Clairmont, A. R., Jr., "Deflagration-to-Detonation Transition Studies of Porous Explosive Charges in Plastic Tubes," in *Proceedings of Seventh Symposium* (*International) on Detonation*, NSWC MP 82-334, Naval Surface Warfare Center, 1982, pp. 119-138.

5. Green, L. G., James, E., Lee, E. L., Chambers, E. S., Tarver, C. M., Westmoreland, C., Weston, A. M., Brown, B., "Delayed Detonation in Propellants from Low Velocity Impact," in *Proceedings of Seventh Symposium (International) on Detonation*, NSWC MP 82-334, Naval Surface Warfare Center, 1982, pp. 256-264.

6. Sandusky, H. W., Coffey, C. S., and Liddiard, T. P., "Rate of Deformation as a Measure of Reaction Threshold in Energetic Materials," in *Mechanical Properties of Materials at High Rates of Strain*, 1984, Conference Series No. 70, The Institute of Physics, Bristol and London, pp. 373-380.

7. Sandusky, H. W., Liddiard, T. P., Bernecker, R. R., Glancy, B. C., Clairmont, A. R., Jr., "Dynamic Compaction of Porous Beds," in *The High Energy Propellant Safety (HEPS) Program Highlights*, CPIA Publication 456, Vol. I, 1987, pp. 163-184.

8. Sandusky, H. W., Elban, W. L., Kim, K., Bernecker, R. R., Gross, S. B., Clairmont, A. R., Jr., "Compaction of Porous Beds of Inert Materials," in *Proceedings of Seventh Symposium (International) on Detonation*, NSWC MP 82-334, Naval Surface Warfare Center, 1982, pp. 843-856.

9. Sandusky, H. W., Bernecker, R. R., and Clairmont, A. R., Jr., *Dynamic Compaction of Inert Porous Beds*, NSWC TR 81-97, Naval Surface Warfare Center, 31 Oct 83.

10. Sandusky, H. W., Elban, W. L., and Liddiard, T. P., "Compaction of Porous Beds," in *Shock Waves in Condensed Matter - 1983*, Asay, J. R., Graham, R. A., and Straub, G. K., Eds., North Holland, Amsterdam, 1984, pp. 567-570.

11. Sandusky, H. W. and Liddiard, T. P., *Dynamic Compaction of Porous Beds*, NSWC TR 83-246, Naval Surface Warfare Center, 26 Dec 1985.

12. Sandusky, H. W., Glancy, B. C., Campbell, R. L., Krall, A. D., Elban, W. L., and Coyne, P. J., Jr., “Compaction and Compressive Reaction Studies for a Spherical, Double-Base Ball Propellant,” in *Proceedings of the 25th JANNAF Combustion Meeting*, CPIA Publ. 498, Vol. I, 1988, pp. 83-94.

13. Glancy, B. C., Sandusky, H. W., and Krall, A. D., “Dynamic Compaction and Compressive Reaction Studies for a Single-Base Ball Propellant,” in *Proceedings of the 1989 JANNAF Propulsion Systems_Hazards Subcommittee Meeting*, CPIA Publ. 509, Vol. I, 1989, pp. 37-46.

14. Glancy, B. C., Sandusky, H. W., Miller, P. J., and Krall, A. D., “Dynamic Compaction and Compressive Reaction Studies for Single and Double-Base Ball Propellants,” in *Proceedings of Ninth Symposium (International) on Detonation*, OCNR 113291-7, Office of the Chief of Naval Research, Vol. I, 1991, pp. 340-353.

15. Sandusky, H. W. and Bernecker, R. R., “Compressive Reaction in Porous Beds of Energetic Materials,” in *Proceedings of Eighth Symposium (International) on Detonation*, NSWC MP 86-194, Naval Surface Warfare Center, 1986, pp. 881-891.

16. Sandusky, H. W., Elban, W. L., Coyne, P. J., Jr., and Clairmont, A. R., Jr., *Compaction Studies on Cross-Linked High-Energy Propellant Shreds*, NSWC TR 88-124, Naval Surface Warfare Center, 12 Sep 1988.

17. Elban, W. L., Gross, S. B., Kim, K., and Bernecker, R. R., *Quasi-Static Compaction Studies for DDT Investigations: Inert Materials*, NSWC TR 81-113, Naval Surface Warfare Center, 1 Dec 1982.

18. Elban, W. L. and Chiarito, M. A., “Quasi-Static Compaction Study of Coarse HMX Explosive,” *Powder Technology*, Vol. 46, No. 2-3, 1986, pp. 181-193.

19. Elban, W. L., Coyne, P. J., Jr., and Chiarito, M. A., “The Effect of Particle Size on the Quasi-Static Compaction Behavior of Granular HMX Beds,” in *Proceedings of the 1987 JANNAF Propulsion Systems Hazards Subcommittee Meeting*, Vol. I, CPIA Publ. 464, 1987, pp. 61-75.

20. Elban, W. L., “Quasi-Static Compaction Studies for DDT Investigations. Ball Propellants,” *Propellants, Explosives, Pyrotechnics*, Vol. 9, No. 4, 1984, pp. 119-129.

21. Elban, W. L. and Coyne, P. J., Jr., “Quasi-Static Compaction Study of ABL 2523 Casting Powder,” in *Proceedings of the 1986 JANNAF Propulsion Systems Hazards Subcommittee Meeting*, Vol. I, CPIA Publ. 446, 1986, pp. 205-212.

22. Campbell, R. L., Elban, W. L., and Coyne, P. J., Jr., Side-Wall Pressure Measurements in Quasi-Static Compaction of Porous Beds of HMX Powders and ABL 2523 Casting Powder,” in *Proceedings of the 1988 JANNAF Propulsion Systems Hazards Subcommittee Meeting*, Vol. I, CPIA Publ. 477, 1988, pp. 1-15.

23. Elban, W. L., Coyne, P. J., Jr., and Campbell, R. L., “The Effect of Nitroglycerin Content on the Quasi-Static Compaction Behavior of Various Ball Propellants,” *Propellants, Explosives, Pyrotechnics,*” Vol. 16, No. 6, 1991, pp. 255-265.

24. Coyne, P. J., Jr. and Elban, W. L., “A Strain Rate Sensitivity Prediction for Porous Bed Compaction,” in *Shock Waves in Condensed Matter - 1983,* Asay, J. R., Graham, R. A., and Straub, G. K., Eds., North Holland, Amsterdam, 1984, pp. 147-150.

25. Coyne, P. J., Jr., Elban, W. L., and Chiarito, M. A., “The Strain Rate Behavior of Coarse HMX Porous Bed Compaction,” in *Proceedings of Eighth Symposium (International) on Detonation*, NSWC MP 86-194, Naval Surface Warfare Center, 1986, pp. 645-657.

26. Coyne, P. J., Jr., Elban, W. L., and Campbell, R. L., “Reassessment of Stress Relaxation Data Analysis to Yield Dynamic Compaction Predictions,” in *Proceedings of the 1990 JANNAF Propulsion Systems Hazards Subcommittee Meeting,* CPIA Publ. 538, Vol. I, 1990, pp. 117-129.

27. Atwood, A. I. et al., “Permeability and Drag Measurements of Compacted Materials,” in *Proceedings of the 1987 JANNAF Propulsion Systems Hazards Subcommittee Meeting*, CPIA Publ. 464, Vol. I, 1987, pp. 113-125. Additional data are reported in Proceedings of the 1986 and 1989 JANNAF Propulsion Systems Hazards Subcommittee Meetings.

28. Costantino, M. and Tao, W., “Compaction of Non-Consolidated HMX Beds,” in *Proceedings of the 1987 JANNAF Propulsion Systems Hazards Subcommittee Meeting*, CPIA Publ. 464, Vol. I, 1987, pp. 77-91.

29. Jacobs, S. J., Sandusky, H. W., and Elban, W. L., “Quasi-Static Compaction of Porous Propellant Beds. I. Modeling Ball Powder Experiments with Deformed Spheres in a Regular Lattice,” *Powder Technology*, Vol. 89, 1996, pp. 209-217.

30. Carroll, M. M. and Holt, A. C., “Static and Dynamic Pore-Collapse Relations for Ductile Porous Materials,” *J. Applied Physics*, Vol. 43, No. 4, Apr 1972, pp. 1626-1636.

31. Sandusky, H. W., “Compressive Ignition and Burning in Porous Beds of Energetic Materials,” in *Proceedings of the 1983 JANNAF Propulsion Systems Hazards Subcommittee Meeting*, CPIA Publ. 381, Vol. I, 1983, pp. 249-257.

32. Sandusky, H. W. and Bernecker, R. R., “Compressive Ignition and Burning in Porous Beds of High Energy Propellants,” in *Proceedings of the 1984 JANNAF Propulsion Systems Hazards Subcommittee Meeting*, CPIA Publ. 409, Vol. II, 1984, pp. 123-133.

33. Sandusky, H. W. and Bernecker, R. R., “Low Amplitude Shock Initiation of Porous Energetic Materials,” in *Proceedings of the 1986 JANNAF Propulsion Systems Hazards Subcommittee Meeting*, CPIA Publ. 446, Vol. I, 1986, pp. 465-472.

34. Lindstrom, I. E., “Plane Shock Initiation of Porous Tetryl,” *J. Applied Physics*, Vol. 41, No. 1, Jan 1970, pp. 337-350.

35. Kooker, D. E. and Anderson, R. D., “A Mechanism for the Burning Rate of High Density, Porous, Energetic Materials,” in *Proceedings of Seventh Symposium (International) on Detonation*, NSWC MP 82-334, Naval Surface Warfare Center, 1982, pp. 198-215.

36. Baer, M. R., “Numerical Studies of Dynamic Compaction of Inert and Energetic Granular Materials,” *J. Applied Mechanics*, Vol. 55, 1988, pp. 36-43.

37. Kooker, D. E., “A Workshop Summary of Compaction Waves in Granular Material: Numerical Predictions,” in *Proceedings of the 1987 JANNAF Propulsion Systems Hazards Subcommittee Meeting*, CPIA Publ. 464, Vol. I, 1987, pp. 127-138.

38. Kooker, D. E., “A Workshop Summary of Model Predictions of the Piston-Driven-Compaction Experiment,” in *Proceedings of the 1989 JANNAF Propulsion Systems Hazards Subcommittee Meeting*, CPIA Publ. 509, Vol. I, 1989, pp. 13-35. Also see, same title, BRL-TR-3029, Ballistic Research Laboratory, Aug 1989.

39. Kooker, D. E., “Compaction Wave Acceleration in Granular Energetic Material: Simulation with a Reactive Shock Wave Model,” in *Proceedings of Ninth Symposium (International) on Detonation*, OCNR 113291-7, Office of the Chief of Naval Research, Vol. I, 1991, pp. 306-319.

40. Baer, M. R. and Nunziato, J. W., “Compressive Combustion of Granular Materials Induced by Low-Velocity Impact,” in *Proceedings of Ninth Symposium (International) on Detonation*, OCNR 113291-7, Office of the Chief of Naval Research, Vol. I, 1991, pp. 293-305.

41. Price, C. F., Atwood, A. I., and Boggs, T. L., “An Improved Model of the Deflagration-to-Detonation Transition in Porous Beds,” in *Proceedings of Ninth Symposium (International) on Detonation*, OCNR 113291-7, Office of the Chief of Naval Research, Vol. I, 1991, pp. 363-376.

42. Hsieh, T. and Kim, K., “Numerical Simulation of Piston-Driven-Compaction Experiment for TS 3659 Propellant,” in *Proceedings of the 1989 JANNAF Propulsion Systems Hazards Subcommittee Meeting*, CPIA Publ. 509, Vol. I, 1989, pp. 85-93.

43. Krall, A. D. Glancy, B. C., and Sandusky, H. W., “Microwave Interferometry of Shock Waves. I. Unreacting Porous Media,” *J.Applied Physics*, Vol. 47, No. 10, 1993, pp. 6322-6327.

44. Glancy, B. C., Sandusky, H. W., and Krall, A. D., “Hot Spot Density Determination in Propellants and Explosives from Microwave Interferometric Data,” in *Proceedings of the 1990 JANNAF Propulsion Systems Hazards Subcommittee Meeting*, CPIA Publ. 538, Vol. I, 1990, pp. 315-324.

45. Glancy, B. C., Sandusky, H. W., and Krall, A. D., “Microwave Interferometry of Shock Waves. II. Reacting Porous Media,” *J.Applied Physics*, Vol. 47, No. 10, 1993, pp. 6328-6334.

46. Groves, C. L., Sandusky, H. W., Clairmont, A. R., Jr., and Bernecker, R. R., “Flash Radiography Measurements on Confined Porous Beds During Dynamic Loading,” in *Proceedings of the 1986 Flash Radiography Topical*, The American Society for Nondestructive Testing, Inc., Columbus, Ohio, pp. 59-66.

47. Cleaver, H. E., *Pin Switch Circuits Instrument for Microsecond Velocity Measurements*, NSWC MP 88-172, Naval Surface Warfare Center, 8 Sep 1989.

48. Bernecker, R. R., “Deflagration-to-Detonation Transition Process for High-Energy Propellants—A Review,” *AIAA Journal*, Vol. 24, No. 1, Jan 1986, pp. 82-91.

49. McAfee, J. M., Asay, B. W., Campbell, A. W., and Ramsay, J. B., “Deflagration to Detonation in Granular HMX,” in *Proceedings of Ninth Symposium (International) on Detonation*, OCNR 113291-7, Office of the Chief of Naval Research, Vol. I, 1991, pp. 265-279.

50. Dick, J. J., “Measurement of the Shock Initiation Sensitivity of Low Density HMX,” *Combustion and Flame*, Vol. 54, 1983, pp. 121-129.

51. Bernecker, R. R, Clairmont, A. R., Jr., Dick, J. J., and Ramsay, J. B., “Shock Initiation Studies of Damaged and Granulated Energetic Materials,” in *Proceedings of the 1986 JANNAF Propulsion Systems Hazards Subcommittee Meeting*, CPIA Publ. 446, Vol. I, 1986, pp. 479-489.

52. Bernecker, R. R., Sandusky, H. W., and Clairmont, A. R., Jr., “Deflagration-to-Detonation Transition (DDT) Studies of a Double-Base Propellant,” in *Proceedings of Eighth Symposium (International) on Detonation*, NSWC MP 86-194, Naval Surface Warfare Center, 1986, pp. 658-668.

53. Bernecker, R. R., “DDT Studies of a Spherical, Double-Base Ball Propellant,” in *Proceedings of 1987 JANNAF Propulsion Systems Hazards Subcommittee Meeting*, CPIA Publ. 464, Vol. I, 1987, pp. 1-12. Also see “DDT Studies of a High Energy Spherical Ball Propellant,” in *Proceedings of Ninth Symposium (International) on Detonation*, OCNR 113291-7, Office of the Chief of Naval Research, Vol. I, 1991, pp. 354-362.

54. Bernecker, R. R., Price, D., and Sandusky, H. W., “Burning to Detonation Transition in Porous Beds of a High-Energy Propellant,” in *Proceedings of the 16th JANNAF Combustion Meeting*, CPIA Publ. 308, Vol. I, 1979, pp. 51-78.

55. Kooker, D. E., *Modeling of Compaction Wave Behavior in Confined Granular Energetic Material*, BRL-TR-3138, Ballistic Research Laboratory, Aug 1990.

56. Kooker, D. E., *A Reactive Shock Wave Model for Compaction Waves in Granular Energetic Material*, BRL-TR-2945, Ballistic Research Laboratory, Nov 1988.

57. Kooker, D. E., private communication.

58. Hsieh, T. and Kim, K., "Numerical Simulation of Deflagration-to-Detonation Transition for TS 3659 Propellants," in *Proceedings of Ninth Symposium (International) on Detonation*, OCNR 113291-7, Office of the Chief of Naval Research, Vol. I, 1991, pp. 329-340.

59. Green, L. G., Chambers, E. S., and Lee, E. L., "Detonation of Porous, High HMX, Nitroglycerin Containing Propellant by Low Level Shock," in *Proceedings of 19th JANNAF Combustion Meeting*, CPIA Publ. 366, Vol. II, 1982, pp. 217-223.

60. Gibbs, T. R. and Popolato, A., *LASL Explosive Property Data*, Univ. California Press, Berkeley, 1980.

61. Roth, J., "Shock Sensitivity and Shock Hugoniots of High Density Granular Explosives," in *Proceedings of Fifth Symposium (International) on Detonation*, ACR-184, U. S. Government Printing Office, Washington, D. C., 1965, pp. 233-238.

GLOSSARY

p	porous bed pressure from jump calculation (MPa)
p_0	initial porous bed pressure (0.1 MPa)
p_w	bed pressure on inner wall of confining tube (MPa)
p_y	Meyers yield stress, average stress over interparticle contacts in a compacting bed (MPa)
t	time relative to bed impact (μs)
t^*	time relative to onset of detonation ($t - t_D$)
t_D	time to detonation (μs)
u	particle velocity (m/s)
v_p	piston velocity just prior to bed impact (m/s)
x	distance relative to impacted end of bed (mm)
x^*	distance relative to onset of detonation ($x - x_D$)
x_D	distance to detonation (mm)
Al	aluminum
AP	ammonium perchlorate
CGC	cold gas compaction
DDT	deflagration-to-detonation transition
HMX	cyclotetramethylenetetranitramine
HTPB	hydroxyterminated polybutadiene
IDC	ignitor driven compaction
IR	infrared
L	porous bed length (mm)
LSGT	large scale gap test
MI	microwave interferometer
NC	nitrocellulose
NG	nitroglycerin
PBX	plastic-bonded explosive
PDC	piston driven compaction
PETN	pentaerythritol tetranitrate
RDX	cyclotrimethylenetrinitramine
SCW	strong compressive wave
SDT	shock-to-detonation transition
TMD	theoretical maximum density at standard pressure and temperature (g/cc)
%TMD	percent theoretical maximum density, volume percentage occupied by solid
$\%TMD_o$	initial %TMD for a porous bed
U	compaction front velocity (m/s)
Δt	time between bed impact and detection of reaction (μs)
τ_i	average axial solid stress, 100p/%TMD (MPa)
1-D	one-dimensional

This page intentionally left blank.

DISTRIBUTION

ADMINISTRATOR
DEFENSE TECH INFO CTR
ATTN DTIC-OCP
8725 JOHN J KINGMAN RD STE 0944
FT BELVOIR VA 22060-6218 1

JHU/CPIA
ATTN SECURITY OFFICER
10630 LITTLE PATUXENT PKWY STE 202
COLUMBIA MD 21044-3200 1

NAVAL SEA SYSTEMS COMMAND
ATTN CODE 53M (R. BOWEN)
2531 JEFFERSON DAVIS HWY
ARLINGTON VA 22245-5160 1

NAVAL SEA SYSTEMS COMMAND
ATTN CODE 53M (D PORADA)
2531 JEFFERSON DAVIS HWY
ARLINGTON VA 22245-5160 1

OFFICE OF NAVAL RESEARCH
BALLSTON TOWER I
ATTN CODE 33 (S LEKOUDIS)
800 NORTH QUINCY STREET
ARLINGTON VA 22217-5660 1

OFFICE OF NAVAL RESEARCH
BALLSTON TOWER I
ATTN CODE 333 (J GOLDWASSER)
800 NORTH QUINCY STREET
ARLINGTON VA 22217-5660 1

OFFICE OF NAVAL RESEARCH
BALLSTON TOWER I
ATTN CODE 333 (J SHORT)
800 NORTH QUINCY STREET
ARLINGTON VA 22217-5660 1

OFFICE OF NAVAL RESEARCH
BALLSTON TOWER I
ATTN CODE 35 (E ZIMET)
800 NORTH QUINCY STREET
ARLINGTON VA 22217-5660 1

OFFICE OF NAVAL RESEARCH
BALLSTON TOWER I
ATTN CODE 351 (J CHEW)
800 NORTH QUINCY STREET
ARLINGTON VA 22217-5660 1

OFFICE OF NAVAL RESEARCH
BALLSTON TOWER I
ATTN CODE 351 (D SIEGEL)
800 NORTH QUINCY STREET
ARLINGTON VA 22217-5660 1

OFFICE OF NAVAL RESEARCH
BALLSTON TOWER I
ATTN CODE 351 (C BEDFORD)
800 NORTH QUINCY STREET
ARLINGTON VA 22217-5660 1

DIRECTOR STRATEGIC SYSTEMS PROGRAMS
ATTN SP 201-27 (E THROCKMORTON)
NEBRASKA AVENUE COMPLEX
287 SOMERS COURT NW SUITE 10041
WASHINGTON DC 20393-5466 1

DIRECTOR STRATEGIC SYSTEMS PROGRAMS
ATTN SP 2211 (M SOTO)
NEBRASKA AVENUE COMPLEX
287 SOMERS COURT NW SUITE 10041
WASHINGTON DC 20393-5466 1

DIRECTOR STRATEGIC SYSTEMS PROGRAMS
ATTN SP 2731 (K KABLER)
NEBRASKA AVENUE COMPLEX
287 SOMERS COURT NW SUITE 10041
WASHINGTON DC 20393-5466 3

DIRECTOR STRATEGIC SYSTEMS PROGRAMS
ATTN SP 27312 (D KENEMUTH)
NEBRASKA AVENUE COMPLEX
287 SOMERS COURT NW SUITE 10041
WASHINGTON DC 20393-5466 1

NAVAL AIR WARFARE CENTER
ATTN CODE 4TL000D (TECHNICAL LIBRARY)
1 ADMINISTRATIVE CIRCLE
CHINA LAKE CA 93555-6001 1

NAVAL AIR WARFARE CENTER
ATTN CODE 4T43A0D (T ATIENZA-MOORE)
1 ADMINISTRATIVE CIRCLE
CHINA LAKE CA 93555-6001 1

NAVAL AIR WARFARE CENTER
ATTN CODE 4T43A0D (H RICHTER)
1 ADMINISTRATIVE CIRCLE
CHINA LAKE CA 93555-6001 1

NAVAL AIR WARFARE CENTER
ATTN CODE 4T4330D (A LINDFORS)
1 ADMINISTRATIVE CIRCLE
CHINA LAKE CA 93555-6001 1

NAVAL AIR WARFARE CENTER
ATTN CODE 4T43OOD (T BOGGS)
1 ADMINISTRATIVE CIRCLE
CHINA LAKE CA 93555-6001 1

NAVAL AIR WARFARE CENTER
ATTN CODE 4T4310D (A ATWOOD)
1 ADMINISTRATIVE CIRCLE
CHINA LAKE CA 93555-6001 1

AIR FORCE RESEARCH LABORATORY
ATTN AFRL/PRSP (C MERRILL)
10 EAST SATURN
EDWARDS AFB CA 93524-7680 1

AIR FORCE RESEARCH LABORATORY
ATTN WL/MNME (G PARSONS)
2306 PERIMETER ROAD, SUITE 9
EGLIN AFB FL 32542-5910 1

ARMY RESEARCH LABORATORY
ATTN AMSRL-WM-BE (D KOOKER)
ABERDEEN PROVING GROUND
ABERDEEN MD 21005-5066 1

ARMY RESEARCH LABORATORY
ATTN AMSRL-WM-TE (P BAKER)
ABERDEEN PROVING GROUND
ABERDEEN MD 21005-5066 1

ARMY RESEARCH LABORATORY
ATTN AMSRL-WM-TE (R FREY)
ABERDEEN PROVING GROUND
ABERDEEN MD 21005-5066 1

LAWRENCE LIVERMORE NATL LAB
ATTN J FORBES
PO BOX 808 L-282 (BLDG 191 HEAF)
LIVERMORE CA 94551 1

LAWRENCE LIVERMORE NATL LAB
ATTN J MAIENSCHEIN
PO BOX 808 L-282 (BLDG 191 HEAF)
LIVERMORE CA 94551 1

LOS ALAMOS NATL LABORATORY
ATTN MAIL STOP C920 (B ASAY)
PO BOX 1663
LOS ALAMOS NM 87545 1

LOS ALAMOS NATL LABORATORY
ATTN MAIL STOP C920 (J MACE)
PO BOX 1663
LOS ALAMOS NM 87545 1

LOS ALAMOS NATL LABORATORY
ATTN MAIL STOP C920 (J RAMSAY)
PO BOX 1663
LOS ALAMOS NM 87545 1

LOS ALAMOS NATL LABORATORY
ATTN MAIL STOP C920 (S SON)
PO BOX 1663
LOS ALAMOS NM 87545 1

SANDIA NATIONAL LABORATORIES
ATTN DEPT 9100 MS 0834 (M BAER)
ALBUQUERQUE NM 87185 1

SANDIA NATIONAL LABORATORIES
ATTN DEPT 9116 MS 0836 (E HERTEL)
ALBUQUERQUE NM 87185 1

SANDIA NATIONAL LABORATORIES
ATTN DEPT 9112 MS 0834 (A RATZEL)
ALBUQUERQUE NM 87185 1

ATLANTIC RESEARCH CORP
ATTN MS 252/0 (K GRAHAM)
5945 WELLINGTON RD
GAINSVILLE VA 20155-1699 1

ALLIANT TECHSYSTEMS
ATTN MS-A1 (R MENK)
4100 SOUTH 7900 WEST
MAGNA UT 84044 1

ALLIANT TECHSYSTEMS
ATTN MS-A1 (D STEPHENS)
4100 SOUTH 7900 WEST
MAGNA UT 84044 1

ALLIANT TECHSYSTEMS
ATTN MS-X7H7 (A BUTCHER)
4100 SOUTH 7900 WEST
MAGNA UT 84044 1

ALLIANT TECHSYSTEMS
ATTN MS-X7H7 (N ROBINSON)
4100 SOUTH 7900 WEST
MAGNA UT 84044 1

LOCKHEED MARTIN SPACE SYSTEMS CO
SUNNYVALE OPERATIONS BLDG B157
ATTN O/L2-60 (T JARYMOWYCZ)
1111 LOCKHEED MARTIN WAY
SUNNYVALE CA 94089 1

LOCKHEED MARTIN SPACE SYSTEMS CO
SUNNYVALE OPERATIONS BLDG B157
ATTN O/L2-70 (E MATHESON)
1111 LOCKHEED MARTIN WAY
SUNNYVALE CA 94089 1

LOCKHEED MARTIN SPACE SYSTEMS CO
SUNNYVALE OPERATIONS BLDG B157
ATTN O/83-02 (J ROSENBERG)
1111 LOCKHEED MARTIN WAY
SUNNYVALE CA 94089 1

DEFENSE THREAT REDUCTION AGENCY
LAUNCH MONITORING DIVISION
ATTN B GLANCY
400 ARMY NAVY DRIVE SUITE 300
ARLINGTON VA 22202-2803 1

SRI INTERNATIONAL
ATTN AF238 (J COLTON)
333 RAVENSWOOD AVE
MENOL PARK CA 94025-3493 1

R BERNECKER
204 PEWTER LANE
SILVER SPRING MD 20905 1

A KRALL
703 McCRONE DRIVE
CROWNSVILLE MD 21032-1211 1

Internal

TDD (S MITCHELL)	1
6210 (T SMITH)	1
8230	1
840L (LIBRARY)	1
90C2 (A DUONG)	1
90B (R DOHERTY)	1
90D (A STERN)	1
920	1
920C3 (C COFFEY)	1
9220 (R LEE)	1
9220V (V JOSHI)	1
9230 (H SANDUSKY)	10
9230A (G CHAMBERS)	1
9230E (G SUTHERLAND)	1
9230G (R GUIRGUIS)	1
9230K (E LEMAR)	1
9230L (J KELLEY)	1

This page intentionally left blank.